AGU PUBLICATIONS

JGR

Journal of Geophysical Research: Solid Earth

RESEARCH ARTICLE
10.1002/2016JB013394

Special Section:
Slow Slip Phenomena and Plate Boundary Processes

Surface creep on the North Anatolian Fault at Ismetpasa, Turkey, 1944–2016

Roger Bilham[1], H. Ozener[2], D. Mencin[1,3], A. Dogru[2], S. Ergintav[2], Z. Cakir[4], A. Aytun[5], B. Aktug[5], O. Yilmaz[2], W. Johnson[3], and G. Mattioli[3]

[1]CIRES and Department of Geological Sciences, University of Colorado, Boulder, Colorado, USA, [2]Geodesy Department, Kandilli Observatory and Earthquake Research Institute, Bogazici University, Istanbul, Turkey, [3]UNAVCO, Boulder, Colorado, USA, [4]Department of Geology, Istanbul Technical University, Istanbul, Turkey, [5]Department of Geophysical Engineering, Ankara University, Ankara, Turkey

Abstract We reevaluate the 72 year history of surface slip on the North Anatolian Fault at Ismetpasa since the $M_w = 7.4$ 1944 Bolu/Gerede earthquake. A revised analysis of published observations suggests that days after the earthquake the fault had been offset by 3.7 m and 6 years later by an additional 0.74 m. Creep was first recognized on the fault in 1969 as a 0.13 m offset of a wall constructed in 1957 that now (2016) has been offset by 0.52 m. A carbon rod creep meter operated across the fault in the past 2 years confirms results from an invar wire creep meter operated 1982–1991 that surface slip is episodic. Months of fault inactivity are interrupted by slow slip ($\leq$10 μm/d) or multiple creep events with cumulative amplitudes of 2–10 mm, durations of several weeks, and with slip rates briefly exceeding >2.5 mm/h. Creep events accommodate 80% of the surface slip and individually release $\approx 10^{-6}$ shear strain on the flanks of the uppermost 3–7 km of the fault. GPS and interferometric synthetic aperture radar methods yield a current fault slip rate of 7.6 ± 1 mm/yr suggesting that creep meters incompletely sample the full width of the surface shear zone. The slip rate has slowed from >10 mm/yr in 1969 to 6.1 mm/yr at present, 4.65 mm/yr of which appears to be due to steady interseismic creep driven by plate boundary stressing rates. We calculate that a further 1 m of aseismic surface slip will precede the next major earthquake on the fault assuming an ≈ 260 year main shock recurrence interval on this segment.

Key Points:
- Afterslip decayed rapidly in the first two decades following the 1944 M_w=7.4 Bolu earthquake, and surface slip is now driven almost entirely by plate boundary shear stress
- Eighty percent of surface creep (~ 7 mm/yr) on the North Anatolian Fault near Ismetpasa occurs as creep events in the top 5 km
- Creep events with 2-10 mm amplitudes increment stress in the upper 5 km of the Anatolian Fault at ~ 8 month intervals

Supporting Information:
- Supporting Information S1
- Data Set S1
- Data Set S2

Correspondence to:
R. Bilham,
bilham@colorado.edu

Citation:
Bilham, R., et al. (2016), Surface creep on the North Anatolian Fault at Ismetpasa, Turkey, 1944–2016, *J. Geophys. Res. Solid Earth*, *121*, 7409–7431, doi:10.1002/2016JB013394.

Received 23 JUL 2016
Accepted 28 SEP 2016
Accepted article online 30 SEP 2016
Published online 25 OCT 2016
Corrected 1 DEC 2016

This article was corrected on 1 DEC 2016. See the end of the full text for details.

1. Introduction

The North Anatolian Fault in Turkey is one of several major transform faults known to slip both in earthquakes and, in some segments, aseismically in the form of surface and subsurface creep [*Barka*, 1996]. The discovery of surface creep was made accidentally during a 1969 field trip to inspect the surface rupture of the 1944 $M_w = 7.3$ Bolu/Gerede earthquake. Clarence Allen, Nicholas Ambraseys, and Alkut Aytun were among the participants of this April 1969 field trip, and each published photographs subsequently documenting evidence for fault creep near the railway station of Ismetpasa (Figure 1). They reported that the eastern wall of a road maintenance compound had been offset by 24 cm [*Ambraseys*, 1970] or 18 cm [*Aytun*, 1982] in a dextral sense by aseismic slip in the 13 years since its construction in April 1957. The aseismic slip rates determined from these approximate numbers for the interval 1957–1969 were 1.5–2 cm/yr, a faster rate than recorded by a 155 m aperture geodetic alignment array (≈10 mm/yr) measured periodically in the following decade by *Aytun* [1982] suggesting that the 1957–1969 offset may have captured rapid afterslip following the 1944 earthquake, the $M_w = 6.9$ earthquake in 1951 [*Eyidogan et al.*, 1991], or the $M_s = 7.1$ Abant/Bolu earthquake of 25 May 1957. An ≈ 800 m fault-normal, 1.2 km along-strike, trilateration/triangulation network measured between 1972 and 1980 also revealed rates of ≈ 10 mm/yr [*Eren*, 1984], a rate that was adjusted to 9.6 mm/yr by the incorporation of a further decade of data [*Deniz et al.*, 1993]. For part of this time (1982–1990) a U.S. Geological Survey-designed creep meter installed near the wall recorded a slower rate of 7.4–7.7 mm/yr [*Altay and Sav*, 1991]. With the development of GPS, interferometric synthetic aperture radar (InSAR), and LIDAR, numerous investigations have confirmed rates of 6–11 mm/yr and have mapped the spatial location and depth distribution of aseismic slip along the fault [*Çakir et al.*, 2005; *Ozener et al.*, 2013; *Kaneko et al.*, 2013; *Cetin et al.*, 2014].

The early reports of a significant slowing in creep rate over decades suggested that slip processes at Ismetpasa were initiated as afterslip following the 1944 $M_w = 7.3$ Bolu/Gerede earthquake [*Ayhan and Kocyigit*, 2010; *Çakir et al.*, 2005]. In this article we show that these earliest estimates of slip between 1957

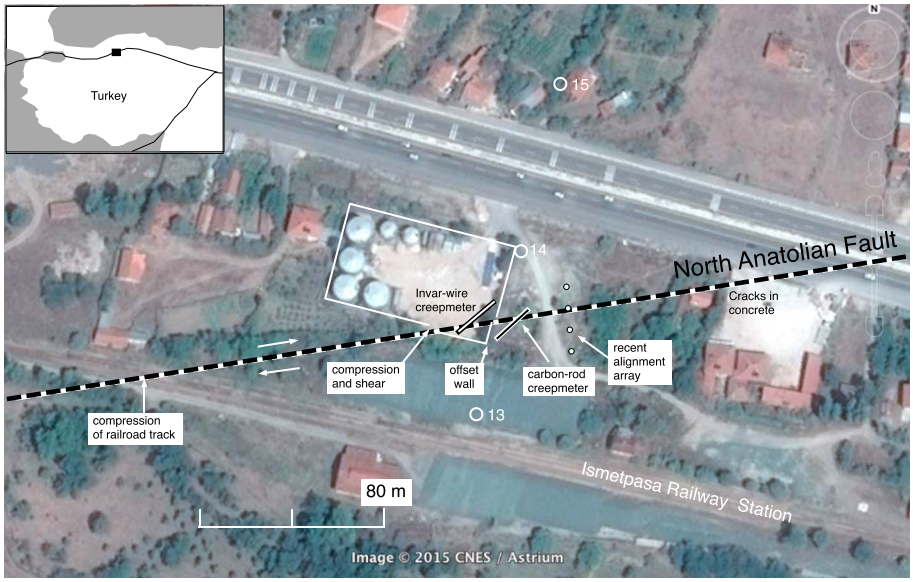

Figure 1. Google Earth view of the Ismetpasa maintenance yard showing the North Anatolian Fault and locations of invar and carbon fiber creep meters (40.870°N, 36.625°E). Nearby geodetic alignment array points 13–15 [*Aytun*, 1982] and the eastern wall of the maintenance yard cross the fault at 66°. The railroad crosses the fault at 24° in compression and has required occasional realignment and shortening to accommodate aseismic fault creep.

and 1969 were inadvertently too large, and that this has influenced subsequent interpretations of afterslip on the fault. Photographs of the offset wall taken throughout the past 59 years indicate that slip rates reduced from ≈ 10 mm/yr in 1969 to less than 7.5 mm/yr currently.

In contrast to these inflated estimates of 1957–1969 afterslip, we deduce that estimates of coseismic slip and pre-1957 afterslip were considerably underestimated. Following the 1944 earthquake and prior to construction of the wall in 1957, two offsets of the adjacent 1934 railroad track were reported: The first estimate of 1.5 m related to repairs to the railroad track after the earthquake in 1944 and the other in 1950 of 30 cm related to the removal of a growing kink in the track caused by afterslip. To reconcile this 1.8 m of cumulative postseismic railroad offset with the 5 ± 1 m post-1944 offsets of cultural features evident nearby [*Kondo et al.*, 2010], we conclude that the 24° obliquity of the railroad track was not taken into account and that dextral fault offset amounted to 4.4 m.

Continuous slip measurements across the fault at Ismetpasa recorded in the 1980s and in the past 2 years reveal episodic creep—slip quiescence interrupted by brief intervals of slow steady creep at 2–5 mm/yr or sudden multiple creep events with initial rates of slip exceeding 3.5 mm/h. The episodic nature of surface slip means that geodetic observations undertaken at intervals of less than several years may yield higher or lower rates due to the existence of infrequent creep events on the fault with cumulative amplitudes of more than 15 mm in 2 months [e.g., *Kutoglu et al.*, 2010]. Creep meters installed across the fault record lower rates than those recorded by the wall or by geodetic methods, due to their incomplete sampling of the ≈ 12 m wide shear zone centered on the fault.

The existence of steady creep on the North Anatolian Fault since ≈ 1980 confirms the similarity of the central Anatolian and San Andreas faults that has been remarked upon elsewhere [*Allen*, 1982; *Kaneko et al.*, 2013; *Bohnhoff et al.*, 2016]. Afterslip followed on the North Anatolian Fault was also documented following the *M*7.4 1999 Izmit earthquake [*Ergintav et al.*, 2009; *Çakir et al.*, 2003, 2012].

The article first presents a precise analysis of extant photographs at Ismetpasa to develop the record of long-term (1957–2016) slip and concatenates it with several previous studies of fault slip in the time domain. This differs from previous studies of creep at Ismetpasa that have considered aseismic slip in the velocity domain. Data from continuous measurements of aseismic slip at Ismetpasa using Invar and carbon fiber creep meters are then analyzed to distinguish both steady state and episodic components of surface creep to deduce the depth range over which each occurs. Finally, we develop an afterslip history between 1944

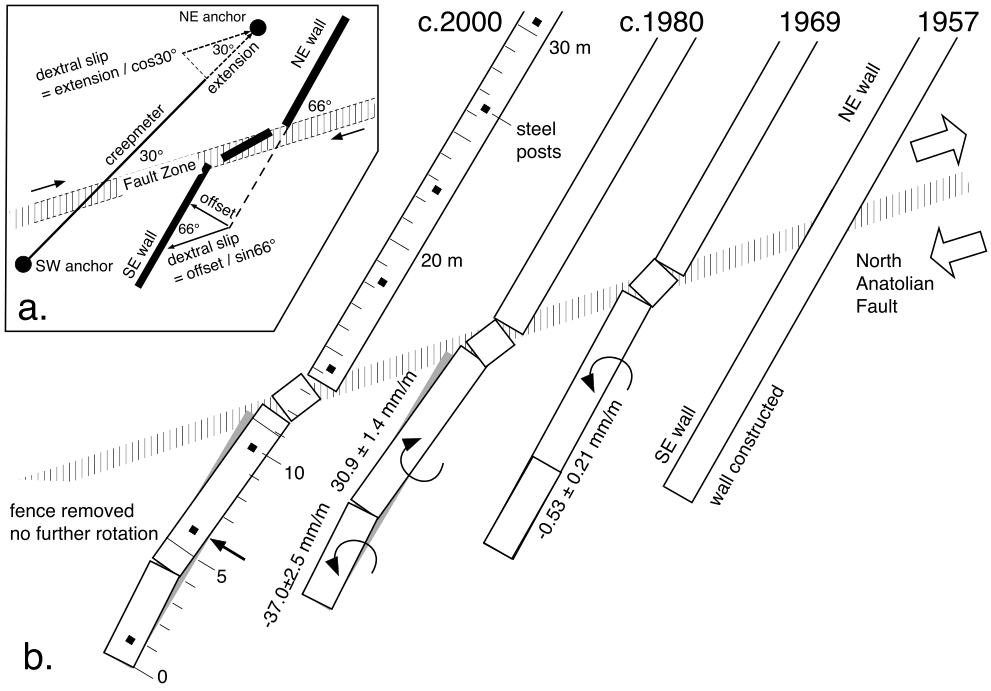

Figure 2. (a) Relations between dextral slip, wall offset, and creep meter extension. (b) In 1970 a chain-link fence was fastened to the capstone of the wall, which caused the progressive clockwise rotation of the southernmost 11.7 m of the concrete cap from the underlying wall. Measurements in 2016 confirm that the two halves of the underlying wall remain parallel. Rotation of the capstone ceased when the chain-link fence was replaced by a free standing fence inside the wall. Throughout the northern half of the wall the saddle coping presently overhangs the wall by 90.8 ± 8.6 mm to the east. This overhang, when applied to the point where the east edge of the wall and capstone intersect, provides an unambiguous measure of offset for photographs taken from above the wall between 1970 and 2010. In 2016 this point lies midway between the southern end of the wall and the fault offset (indicated by arrow).

and 2016 in an attempt to resolve the transition from afterslip to present-day plate boundary stressing in the context of the earthquake cycle on the Ismetpasa segment of the North Anatolian Fault.

2. The 1957 Wall at Ismetpasa

Our study of surface slip at Ismetpasa was initially motivated by a numerical discrepancy in the 1957–1969 offset of the eastern wall of the maintenance compound where creep was first reported. *Ambraseys* [1970] describes the wall as being initially discovered in April 1969 with an offset of 24 cm, yet during a 14 October 1969 return visit *Aytun* [1982] recorded an offset of only 18 cm. Ambraseys qualified his observation with the statement "… one can debate about the accuracy of this figure…" suggesting that there may have been some observational discussion in the field. We resolve this measurement uncertainty by examining contemporary photographs using the width of the wall to scale the 1969 offset, which when combined with its azimuth relative to the strike of the fault provides a precise measure of dextral slip.

We describe below how we quantify the offset of the wall from published photographs. The accuracy of the measurements of published photos is limited to 10–15 mm by the resolution of the dot matrix in the printed pages. From Ambraseys's Figure 13, Aytun's Figure 3, and Allen's Figure 5, it is possible to average the measured offset of each side of the wall as 114 ± 15 mm, 119 ± 10 mm, and 122 ± 17 mm, respectively, using the current mean wall width as a scale. The mean 695 ± 21 mm width of the wall's saddle-coping capstone is based on the average of 31 measurements in 2016.

To convert photographically determined wall offset to fault-parallel dextral slip, the obliquity of the wall to the fault is required (Figure 2), which was not specified by these early authors except in the form of sketch maps. *Ambraseys*'s [1970, Figure 12] sketch shows the azimuth of the wall as N27°E, and *Aytun*'s [1982, Figure 2] sketch shows it at N24°E. Ambraseys's and Allen's photos of the wall, when projected southward,

Table 1. Estimated and Photographically Quantified Wall Offset and Dextral Slip[a]

Source	Wall Azimuth	Fault Strike	Obliquity	Published (mm)	Photo (mm)	Dextral (mm)	Epoch
Ambraseys [1970, Figure 13]	N27E	N83E	(56°)	240	114 ± 15	126 ± 17	1969.4
Aytun [1982, Figure 3]	N24E	N82E	(58°)	180	119 ± 10	130 ± 12	1969.8
Allen [1982, Figure 5]	N15E	N82E	66°	-	122 ± 17	134 ± 19	1969.4
Allen 1969 north photo[a]	-	-	66°	-	117 ± 6	128.6 ± 7	1969.4
Allen 1969 south photo[a]	-	-	66°	-	109 ± 6	119.4 ± 7	1969.4
Weighted 1969 offset[a]						125.4 ± 4.3	1969.4
Bilham 1970 north photo	-	-	-	-	147 ± 25	161 ± 30	1970.7
Aytun [1982, Figure 4]	-	-	-	-	186 ± 13	204 ± 14	1978.7
Thatcher 1980 photo	-	-	-	-	214 ± 20	234 ± 22	1980.4
Jackson 1984 photo 1	-	-	-	-	252 ± 15	276 ± 20	1984.4
Jackson 1984 photo 2	-	-	-	-	247 ± 30	270 ± 32	1984.8
Şaroğlu and Barka [1995]	-	-	-	400	-	400 ± 50	1995.5
Lidar [2007]	-	-	-	-	416 ± 10	455 ± 12	2007.7
21 May 2014, 2.8 mm lens	N15 ± 0.5°E	N81 ± 2E	66 ± 2.5°		465 ± 25	509 ± 27	2014.4
Lidar 2007	-	-	-	-	500 ± 30	547 ± 35	2015.6
25 April 2016, 20 cm lens[b]	-	-	-		482 ± 10	528 ± 11	2016.3
25 April 2016, 50 mm lens[b]	-	-	-	-	458 ± 10	504 ± 11	2016.3
Weighted 1957–2016 offset						516 ± 15	2016.3

[a]Photographs mentioned in column 1 are reproduced in the electronic supporting information
[b]From least squares fits to east and west edges of the capstone.
[c]Least squares fits to east edge of wall. The LIDAR 2007 data are from *Karabacak et al.* [2011]. The 2015 Lidar data were newly obtained but are as yet unpublished. Figure numbers in parentheses in column 1 refer to those in cited publications. The penultimate column indicates dextral slip from wall offset assuming 66° wall/fault obliquity.

intersect the approximate center of a house 100 m south of the fault. This house is visible both on the 26 August 1965 Corona 2 m resolution imagery (Scene DS1023-2135DF107) and on Google Earth 2013 imagery, indicating that the azimuth of the wall was then, and is now, N15 ± 2°E. Although Ambraseys's and Aytun's azimuths may thus be discarded, their implied azimuths may have influenced the reported estimates of dextral slip calculated from their measured offsets of the wall. Alternatively, the published values for offset may have been influenced from considerations of the overthrust southwest wall whose offset was obscured by crushing and which, following early repairs, has now been replaced by a drain.

To estimate the local strike of the fault, we measured the fault azimuth 2 km eastward from Ismetpasa to an offset cowshed wall at Hamamli (N83.5°E), and 2.2 km westward (N78°W) to an offset curb at a petrol station, and adopted a mean strike of the fault at Ismetpasa of N81°E with an uncertainty of about 2° due to the local change in strike of the fault. The obliquity of the fault to the wall (66°) requires the observed offsets of the wall to be multiplied by 1/sin(66) = 1.09 ± 0.02 (Figure 2). Hence, the above derived offsets from analysis of the wall yield dextral slip estimates of 126, 130, and 134 mm, respectively (Table 1), significantly less than the 240 mm dextral slip on April 1969 reported by Ambraseys but close to Aytun's 180 mm estimate made in October 1969. These discrepancies are too large to be accounted for by the apparent errors in wall obliquity attributable to these early reports. Ambraseys would have needed an obliquity of 26°, but his sketch indicates 56° (close to the complementary angle). Aytun would have needed an obliquity of 39°, but his sketch indicates 58°. An error in our assumed width of the concrete capstone to the wall (caused by possible repairs since 1969) would scale both values linearly; however, cracks in the 1969 photographs of the concrete saddle coping that caps the masonry wall are evident to this day, and uniquely identifiable, fieldstone blocks within the wall remain in their original positions. We conclude that the present wall has not been reconstructed in the past five decades.

Because the accurate measurement of the offset in 1969 is central to constraining early creep rates at Ismetpasa we explain our analysis in detail. Two of the original May 1969 35 mm negatives, provided by Clarence Allen, were scanned at 4000 dpi (6 μm pixel sampling of the 35 mm image) and loaded into a standard graphic analysis software (*Eazydraw*) order to numerically quantify the deviation of each edge of the wall from a straight line at ≈ 1 m intervals. The following procedure was adopted to obtain offsets with uniform sample spacing along the wall from oblique perspective photographs (Figure 4). Straight lines were first aligned by eye with each edge of the wall converging at a vanishing point on the eye-line horizon. Points of equal wall width were next constructed horizontally across the digitized photograph to act as a template for lines converging at an arbitrary, but spatially separated, second vanishing point, also on the eye-line

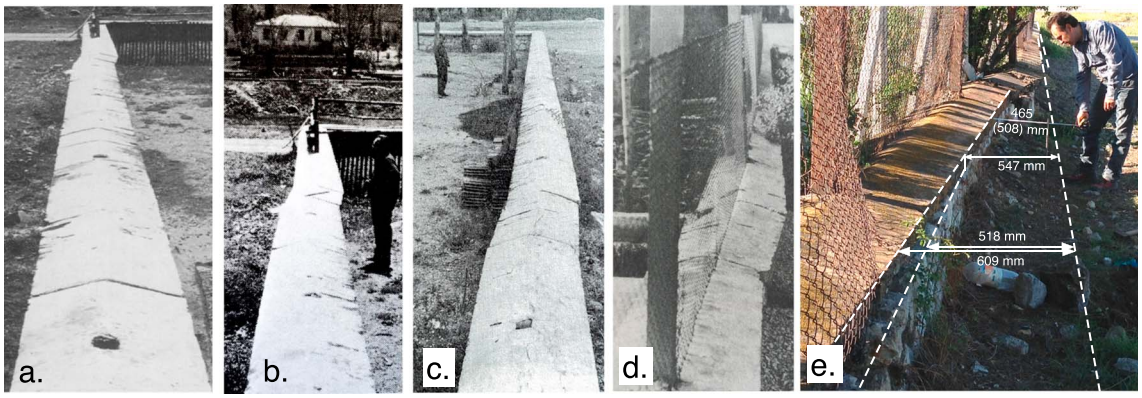

Figure 3. Published photographs of the Ismetpasa wall. (a) *Ambraseys* [1970] view south April 1969. (b) *Allen* [1982] view south April 1969. (c) View north [*Aytun*, 1982] 14 Oct 1969 and (d) view north [*Aytun*, 1982] 11 July 1978. The house visible in Figure 3b can be readily identified in 1965 and 2013 satellite imagery and constrains the 1969 azimuth of the wall to N15°E. (e) View north, May 2014. Distances from a projected alignment to the northern half of the wall to the southern wall and its damaged capstone are indicated where capstone rotation has exposed the top of the wall.

horizon. The intersection of these converging lines with the constructed line following the east side of the wall identified the locus of equal distances along the wall for measurements of wall width and offset. The distances from the subpixel east and west edges of the wall to the guide lines (x_e and x_b) were measured at each of these points and an average offset derived in arbitrary units on the screen. This mean offset was converted to a dimensionless ratio by dividing each average by the local wall width measured on the photographic image (x_{wall}). To convert these photographically derived ratios to millimeters of true local offset, we multiplied each derived ratio by the mean wall width measured directly in 2016 (695 mm). The correct positioning of the artificial eye horizon and the two wall-parallel reference lines is somewhat subjective but does not influence the accuracy because linear trends in the numerical series are removed prior to estimating fault offset, as explained below.

To determine the offset of the wall where it crosses the fault, we fit straight lines in a least squares sense to the north and south halves of the numerical series derived above. A <2 mm one standard deviation misfit was typically obtained for each of these alignments. The lateral separation of these two lines provides an objective offset, but since the two lines are not precisely parallel, the offset depends on the point chosen to evaluate it. The chosen point is the midpoint of the shear zone of the fault, ≈12 m from the southern end of the wall. The two original 35 mm photographs yielded dextral offsets of 129 ± 6 mm (viewed north) and 119 ± 6 mm (viewed south), a difference that we attribute to local roughness in the edge of the capstone. The average derived from scanned images of the three published 1969 photographs was 130 ± 9 mm (Table 1).

For the 2016 data, and for all inferred offsets 1970–2016, the east edge of the capstone south of the fault is a misleading indication of offset because it has been pulled clockwise relative to body of the wall by the superstructure of the steel chain-link fence across the fault (Figures 2 and 3). To correct for capstone rotation in 2016, we subtracted the measured eastward overlap, and a short westward underlap (see Figure 3e), of the east edge of the capstone from the underlying wall at 1 m intervals along the entire wall (supporting information Table S1) and subtracted this from the photographically derived offsets of the eastern edge of the capstone. A least squares fit to the resulting series yields a measure of the straightness and azimuth of the wall both south and north of the fault, independent of capstone misalignment. The formal uncertainty in the offset of the resulting north and south least squares fits was ±2.5 mm, but we recognize that the accuracy of the conversion from capstone offset to wall offset depends on the value of the original 1957 overlap south of the fault for which we have no direct measure. To estimate this, we determined the mean and standard deviation of the eastward overlap of the capstone on the northern half of the wall (90.8 ± 8.6 mm) and derived a combined offset and uncertainty of 90.8 ± 11 mm. This value represents the correction needed to compare the eastern edge of the northern *capstone*, with the eastern edge of the underlying southern *wall* to overcome errors in cap rotation. LIDAR scans of the wall taken in 2007 and 2009 [*Karabacak et al*., 2011] indicate that the average roughness of the fieldstone wall exceeds the uncertainty attributed to the top edge of the wall alone (Figure 4c). Several photographs of the 2016 offset were analyzed yielding slightly different values depending on whether points closer than 3 m to the fault were included in the analysis (Table 1).

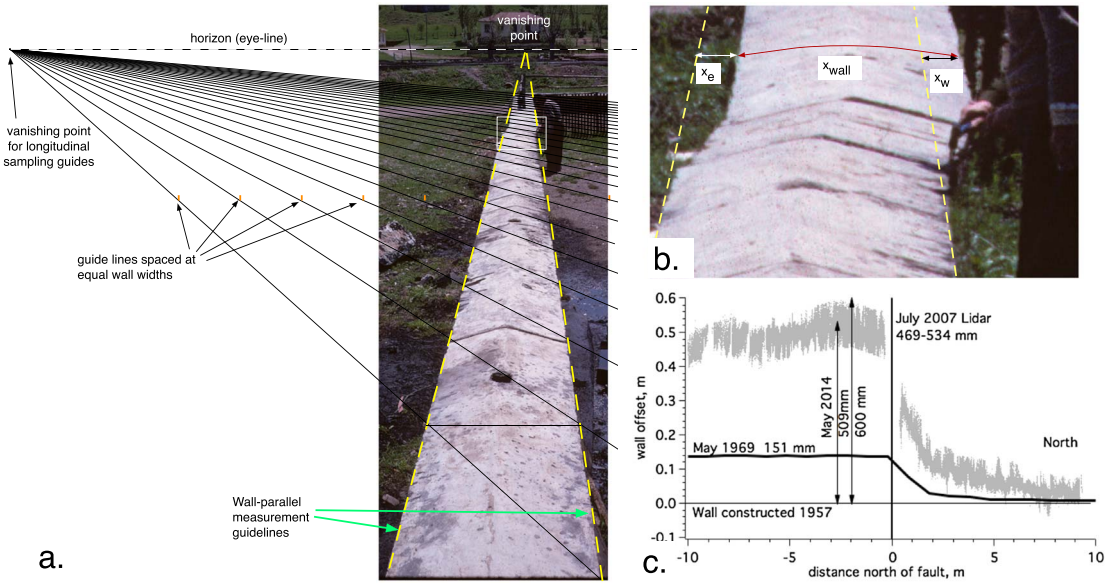

Figure 4. (a) Geometrical projection used for photo analysis of the Ismetpasa wall showing (b) enlarged view of fault offset and measured parameters: x_e = offset east edge, x_w = offset west edge, and x_{wall} = horizontal width of wall colinear with x_e and x_w. At each longitudinal point the dimensionless ratio $(x_e + x_w) / (2 \times x_{wall})$ was determined numerically and multiplied by the mean measured wall width (695 mm) to determine the local offset in millimeters. (c) The capstone offset (black line May 1969) is compared with the 2007–2015 LIDAR capstone and wall offset (grey shading indicates point cloud), and offsets identified in Figure 3e.

The wall was surmounted by a brush-thicket fence in 1970, and subsequently by pillars and a chain-link fence, making sequential photographs showing both east and west edges of the wall and the crest of its centerline, similar to those shown in Figures 3a–3d, impossible. Photos in 1970, 1980, and 1984 show only the eastern edge of the wall, and in photographs this is sometimes obscured by weeds and bushes. The photographs (see supporting information) show the wire chain-link fence progressively tensioned by fault slip. The increasing tension eventually resulted in the detachment of the southern capstone from the underlying wall and clockwise rotation of the capstone. Because all photos of the wall were taken from above, they must be corrected for this rotation. In 2016 precise measurements of this rotation indicated that the east edge of the capstone and the east edge of the wall coincide at a point midway between the southern end of the wall but this crossover point is expected to vary with time, because the axis of rotation is near the center of the wall. Where the full width of the wall was not visible, we used the crest of the saddle coping as a linear feature (width/2) to calibrate offset of the eastern edge of the wall or calibrated blemishes in the wall from other photos to scale the offset. A reported offset of 40 cm by *Şaroğlu and Barka* [1995] is not accompanied by a photograph, an uncertainty, or an indication of what obliquity correction was applied, and consequently to this, we assign a large uncertainty (±50 mm). Photographically derived offsets of the wall are listed in Table 1 and are plotted in Figure 5.

LIDAR measurements were obtained in 2007–2009 [*Karabacak et al*., 2011] and also in 2015. These data were decimated by retaining all but the first arriving offsets consisting of a 40 mm wide band describing wall roughness. The residual data were detrended using a least squares fit to data on the northern half of the wall and the offset across the fault measured between points ±3.5 m of the fault. The offsets so determined were assigned uncertainties of 11 mm for 2007 and 35 mm for the 2015 measurement which more comprehensively characterizes the roughness of the northern half of the wall.

The weighted mean of all five 1969 estimates of wall offset is 125.4 ± 4.3 mm yielding a mean 1957–1969 rate of 10.45 ± 0.35 mm/yr. The most reliable measured offset of the wall (avoiding capstone rotation) since then is 516 ± 15 mm derived in 2016, a mean 1957–2016 rate of 8.75 ± 0.09 mm/yr. The formal 1957–2016 rate uncertainty is underestimated in that it does not account for roughness of the underlying wall imaged by LIDAR.

The mean 1969–2016 rate is 8.8 ± 0.3 mm/yr, a 25% slowing in rate compared to pre-1969 rates. The 1957 to 1969 rate lies within the uncertainties of the 10.7 ± 0.7 mm/yr 1969–1979 rate observed by *Aytun* [1982] and the 9.6 mm/yr rate 1972–1990 reported by *Deniz et al*. [1993]. A linear weighted least squares fit to all the

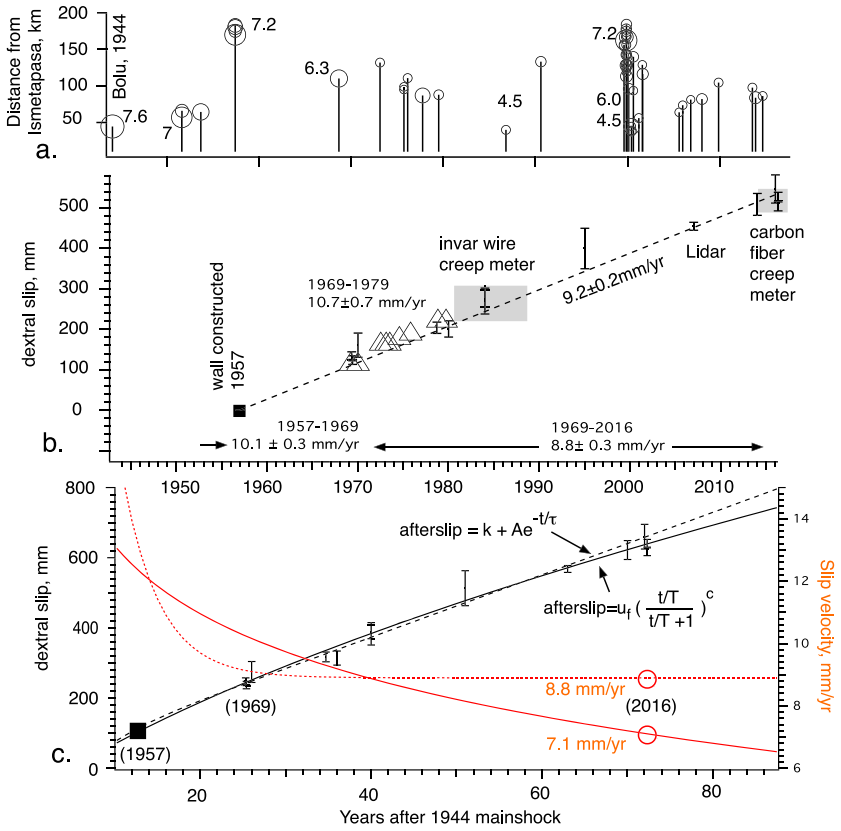

Figure 5. (a) Epicenters of significant earthquakes as a function of distance from Ismetpasa. The Bolu Gerede earthquake occurred 05:22 local time 1 February 1944. (b) Dextral surface creep at Ismetpasa since wall construction in 1957 (Table 1) fit to straight line segments. The weighted least squares fit to all the wall offset data yields 9.2 ± 0.2 mm/yr, but least squares fits to early data yield a higher rate. Triangles indicate 10 years of 155 m aperture alignment array measurements with a mean rate of 10.7 ± 0.7 mm/yr [*Aytun*, 1982], and grey areas indicate the times of operation of continuous creep meters. (c) Synthetic afterslip curves that equally fit the data shown in Figure 5b but predict different early afterslip and cumulative interseismic creep (arbitrary absolute datum). The dashed exponential fit rapidly approaches a linear interseismic slip rate, after an initial decay with an ≈ 10 year decay constant. Present-day velocities predicted by each curve are circled on the slip velocity curves (red).

photographically determined offsets, constrained to pass through the origin (wall construction in 1957), indicates a mean creep rate of 9.2 ± 0.2 mm/yr (Figure 5b).

No perturbations in slip rate are evident in the data following several nearby earthquakes on the fault or the 1999 earthquakes [*Kutoglu et al.*, 2008, 2010]; however, wall offsets are constrained between 1984 and 2007 by a single point in 1995 devoid of a photographic record or stated uncertainty [*Şaroğlu and Barka*, 1995]. We discuss next the occurrence of large creep events recorded by creep meters at Ismetpasa whose unrecorded occurrence would result in apparent accelerations in rate that will have escaped notice in the sparse photographic record.

3. Continuous Measurements of Creep Using Invar and Carbon Rod Creep Meters

In 1982, a 20 m long Invar wire creep meter was installed at Ismetpasa [*Altay and Sav*, 1991]. In their Figure 3 they show the azimuth of the wall as N12°E, the fault as N76°E and their creep meter as N48°E, implying an obliquity of 28° close to the 30° claimed in their text. If we assume that they used uncorrected magnetic bearings to determine azimuths, their corrected wall azimuth (15°E) and their fault strike would be N79°E consistent with that adopted in this article. This would imply that their creep meter azimuth was N51°E, which when combined with our adopted fault strike (N81°E) is consistent with their stated obliquity of 30° (Figure 6).

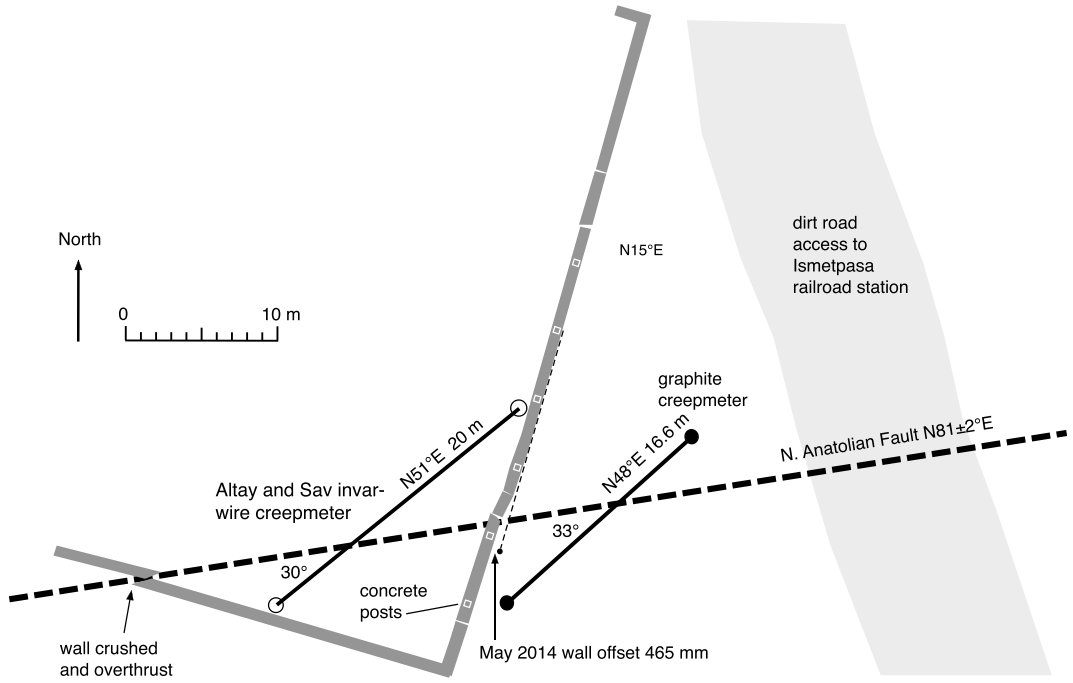

Figure 6. Location of creep meters relative to the 47 m long offset wall discussed in the preceding section.

The Invar wire of the Altay and Sav instrument was freely suspended in a catenary within a buried pipe crossing the fault at a depth of 1.5 m. The wire was anchored at its western end and held in tension at its eastern end by a mass balance rotating on a hinge [*Burford and Harsh*, 1980]. The rotation of the mass was recorded by an LVDT (linear voltage differential transducer) whose voltage output was registered by a strip chart recorder with a chart-recording speed of 15 cm/d, a sample rate of 12 s, and full-scale recording span of approximately 3.3 mm. Mechanical adjustments were required to bring the record back on scale when the 3.3 mm recording range was approached or exceeded, but the absolute datum was simultaneously indicated by means of a scale attached to the rotating mass. Thus, although continuous data were lost on five occasions, the cumulative creep record was preserved by a sequence of manual readings before and after gaps in recording. These manual offsets were not published.

Data from Altay and Sav's Invar wire creep meter are reproduced from their hand-drafted cumulative plot in Figure 7a. A digital listing of these data will be found in the supporting information. The mean dextral slip rate averaged over 8 years is stated to be 7.4–7.7 mm/yr, but a least squares fit to a digitized version of their plotted data yields a rate of 7.34 ± 0.10 mm/yr, possibly resulting from the different temporal sampling adopted in our digitization of their data. The data consist of multiple creep events with amplitudes of up to 2.5 mm separated by intervals of slow creep or zero slip. Infrequent slow sinestral displacements were recorded, presumably due to soil contraction in summer months.

Chart records of four creep events (Figure 7b), which together form part of the largest observed sequence in their data, are reproduced in their article with amplitudes of 0.66 mm to 2.54 mm, with decay time constants of 1–2 h, and with durations of less than 30 h. Throughout their data Altay and Sav recognize a bimodal distribution of creep events, distinguishing between those with amplitudes of <0.7 mm and others with amplitudes of ≥ 1.5 mm. They note periods of steady slow slip on the fault. Some of their events end abruptly, while others continue as slow slip. Operation of the Invar wire creep meter was discontinued as a result of new construction inside the compound.

In May 2014 we installed a carbon fiber rod creep meter outside the compound to the east of the wall (Figures 6 and 8). A continuous 4 mm diameter, 16.5 m long, carbon fiber rod slides within a 12 mm internal diameter, PVC conduit joined with O-ring expansion slip joints buried 33° obliquely across the fault below a depth of 35 cm. The western end of the rod is anchored rigidly to a stainless steel tripod driven to 2 m depth with one vertical rod and two rods inclined at 45° riveted at the top. A second identical buried tripod

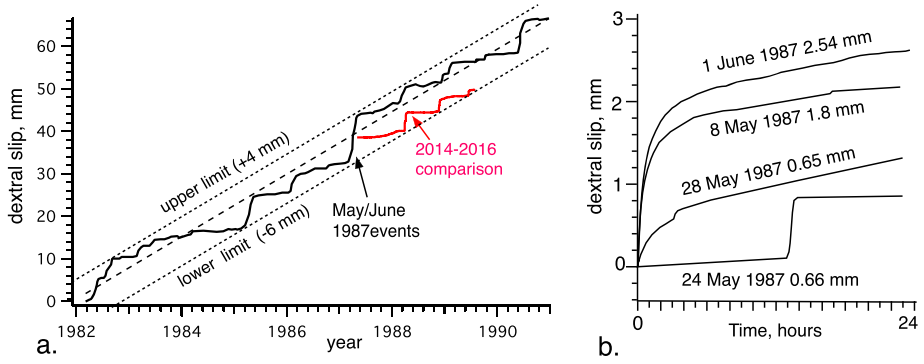

Figure 7. (a) Cumulative creep recorded by *Altay and Sav* [1991] with (b) creep events reproduced from their article. The authors reported a mean creep rate of 7.46–7.7 mm/yr; the dashed least squares fit line shown has slope 7.3 ± 0.1 mm/yr. Creep events occur when surface creep lags 6 mm below the mean creep rate, and the relaxed surface slip state is no more than 4 mm above it. Recent 2014–2016 creep data with arbitrary time and displacement datum are superimposed on the 1987–1989 data for comparison purposes.

arrangement installed 16.6 m to the east on the far side of the fault supports a displacement sensing unit. The free eastern end of the rod is held in tension by a flexible wire fastened to a 4.5 N constant-tension spring motor via a 90° elbow that feeds the wire to the surface (Figure 8). Two transducers measure the extension caused by fault motion: a subsurface 12 mm range LVDT and a Hall effect transducer installed in an electronics housing 50 cm above the surface. The Hall effect rotary transducer is attached to a 100 mm circumference wheel around which the flexible wire is wrapped. The wire is held in tension by a spring motor with a range of approximately 1.5 m. The arrangement is designed so that should the LVDT reach the end of its range, a record of slip of up to 1.5 m is retained by the Hall transducer. Displacement data are recorded along with temperature and battery health information by a 12-bit data logger providing least-count resolutions of 3 μm and 25 μm for the LVDT and Hall effect transducers, respectively. The data are simultaneously converted to dextral slip in millimeters and transmitted via the Iridium satellite with a maximum latency of 30 min. A correction factor for obliquity and sensor calibration (1.271) has been applied to the transmitted data (see supporting information for these digital data) to convert these displacement data to dextral slip (Figure 9), but no other editing was required. In April 2016 a second data logger was added with a 5 s sampling rate to record the details of creep events. This second logger has a memory capacity of 3 weeks and must be downloaded manually before the creep event data are overwritten.

Despite burial at only 35 cm depth, the graphite rod and LVDT sensor are not significantly influenced by annual surface temperature changes of up to 60°C (Figure 9). A periodic daily signal of 0.6 μm/°C is evident

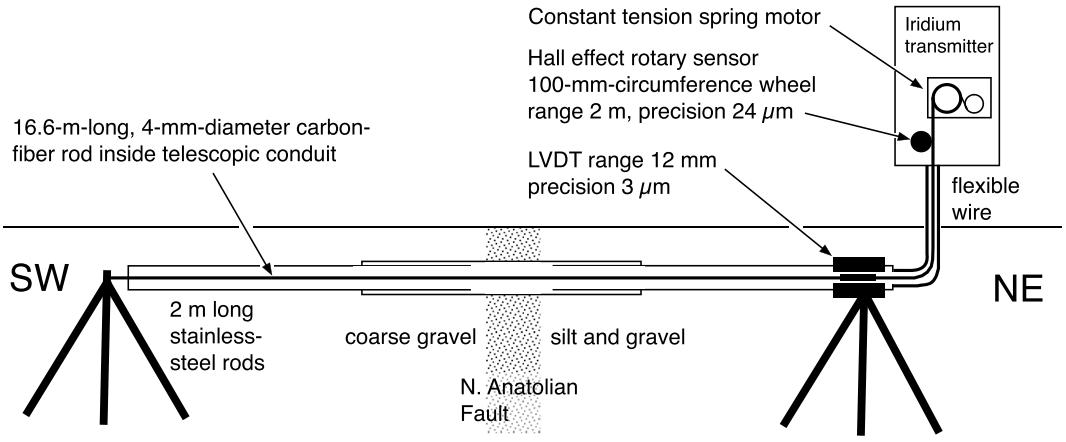

Figure 8. Schematic cross section of the 16.6 m long Ismetpasa creep meter. The rotary sensor is driven by a single turn of stranded stainless steel wire wrapped around a precision 100 mm circumference wheel. The rod slides inside a PVC conduit which results in occasional "stiction" with amplitudes 3–20 μm.

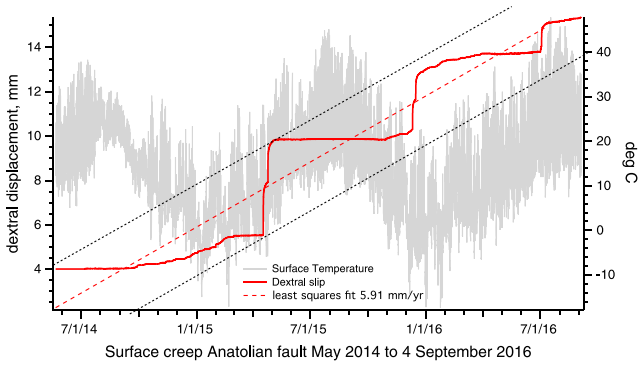

Figure 9. Ismetpasa creep data to May 2014 to September 2016 from the carbon fiber rod creep meter. The trace starts after a ~20 mm Aug–Sep 2013 creep episode reported by [*Rousset et al*., 2016] 10 km to the east of here and stops following a third creep episode that occurred too late for analysis in the current manuscript. The black dashed lines are parallel to, and ±2 mm from, the least squares fit to these data (5.91 ± 0.01 mm/yr). In this time interval the surface trace spends 47% of its time locked and 44% of its time creeping at a slow rate of 3.5 ± 2 mm/yr. This slow slip contributes 25% of the total slip of 10.86 mm in 2 years. The creep trace is insignificantly influenced by environmental temperature effects (the grey trace records 60°C annual, and 5–30°C daily, surface temperature changes).

in the LVDT signal, but this signal is more pronounced (≈100 μm/°C) in the aboveground Hall effect sensor, which is influenced by the mounting arrangement of the solar panel and Iridium transmitter. In August of each year we recorded a 28 μm cumulative slow left-lateral displacement that we attribute to thermoelastic processes similar to the ≈ 0.1 mm left-lateral seasonal signal noted by *Altay and Sav* [1991].

The continuous record from April 2014 to 16 June creep (Figure 9) exhibits the same features as exhibited in the 1982–1990 creep data: periods of no slip are interrupted by slow slip at rates of 2–6 mm/yr, and/or by abrupt creep events, each consisting of a double creep event. In 2015 double creep events were separated by 120–180 h but the larger events evident in Altay and Sav's creep data appear to be separated by several weeks. Amplitudes of individual recent creep events are 1.3–2.5 mm, similar to those recorded in the 1980s.

The creep events in the past 21 months at Ismetpasa have contributed ≈ 7.2 mm of the total of total dextral slip, with the remaining 2.6 mm occurring in the form of slow slip. On the Superstition Hills Fault, California, the existence of slow uneventful slip punctuated by distinct creep events was attributed to a variation in rheology with depth [*Bilham and Behr*, 1992]. Steady slip was considered to be confined to shallow layers within 100 m of the surface, with episodic events occurring between the surface and depths of ≈ 3 km [*Du et al*., 2003; *Wei et al*., 2013]. The recent uneventful creep at Ismetpasa constitutes 27% of the total slip signal. For the 1982–1990 creep data of *Altay and Sav* [1991], we estimate that at least 19% of the total creep comes from slow slip.

In Figure 10 we illustrate the variation of surface slip rate with depth of creep anticipated by an elastic model with imposed regional shear of 2.2×10^{-7}/yr (22 ± 3 mm/yr at ±50 km) [*McClusky et al*., 2000] (24 ± 2 mm/yr) [*Reilinger et al*., 2006] and a shear rate of 22 mm/yr below 10 km depth [*Cetin et al*., 2014]. We used a 3-D boundary element elastic half-space model [*Gomberg and Ellis*, 1994] in which shear tractions are imposed ±50 km from and parallel to a locked vertical fault between a shallow depth *d* and the base of the seismogenic zone D. We varied the depth of the freely slipping frictionless fault above depth, *d*, to quantify the resulting surface slip. *Bohnhoff et al*. [2016] estimate a mean depth, *D*, to the base of the seismogenic zone for the Anatolian Fault of 12–14 km. Assuming a seismogenic depth of 12 km at Ismetpasa, the ≈ 8.8 mm/yr slip rate recorded by the offset wall across the fault in recent decades (Figure 5) corresponds to creep from the surface to 5.5 ± 0.1 km (Figure 10c), similar to that derived from 1992 to 1999 InSAR studies based on a calculated rate of 8 ± 2 mm/yr at Ismetpasa [*Çakir et al*., 2005; *Cetin et al*., 2014]. The creep meter data with its current rate of 5.9 mm/yr suggest that this shallow component of creep now extends to 3.6 km depth and that the 25% contribution from slow slip (Figure 9) is confined to depths shallower than 1.8 km (cf. Figure 8) [*Bilham and Behr*, 1992].

The surface creep rate indicated by creep meter data acquired 2014–2016 (5.9 mm/yr from Figure 9) is lower than that indicated by the interpolated rate from the offset wall (6.1 mm/yr), and 22% slower than that observed from nearby GPS observations 2005–2011 [*Ozener et al*., 2013], but samples an insufficiently long history of slip to be certain of the significance of its mean rate. However, the much longer 8 year long rate measured by the creep meters in the 1980s (7.3–7.7 mm/yr) was then 16% lower than the mean rate recorded geodetically [*Kutoglu and Akcin*, 2006]. We attribute these lower rates to the narrower fault-normal sampling

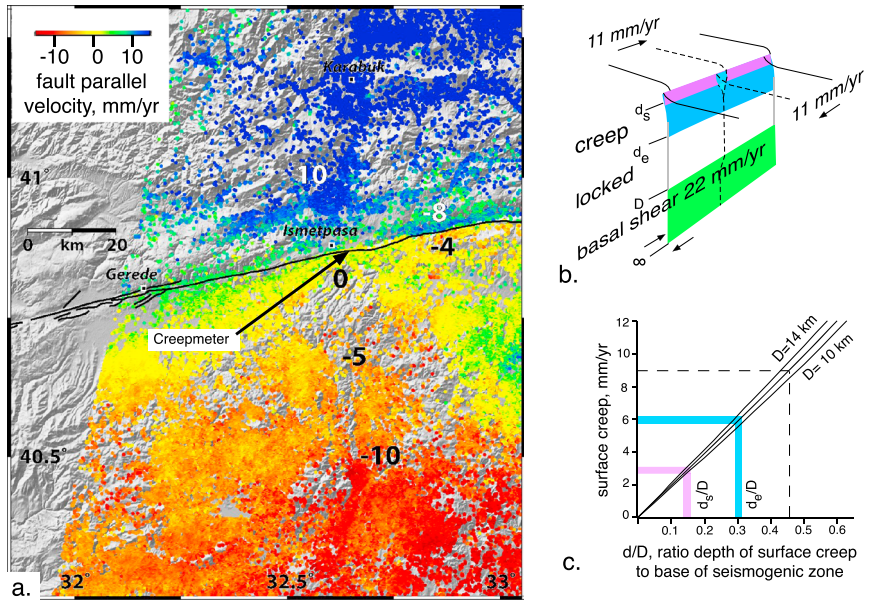

Figure 10. (a) Point InSAR velocity field (2003–2010) from *Cetin et al.* [(2014] with (b) schematic view of steady and episodic creep on fault above the locked seismogenic zone. (c) An elastic model of Figure 10b showing dependence of surface slip rate on the depth of creep for $D = 10$, 12, and 14 km. For the data shown in Figure 9, slow uneventful slip (violet) occurs at depths shallower than $d_s = 1.8$ km, and episodic creep (blue) occurs to a depth of $d_e = 3.6$ km for $D = 12$ km.

aperture of the creep meter (10 m) compared to the deformed width of the wall (≈20 m). Cracks indicating the rotation of wall segments suggest that to completely sample the deforming zone, the length of 30° oblique creep meters would need to be 30 m (Figure 6), which presents difficulties with the current installation, because it would require us to extend the instrument beneath a road.

The lower rate sampled by the creep meters has important implications for the interpretations of fault zone rheology and strain release during creep events. The mean rate measured by the creep meter 1982–1991 (7.6 ± 0.1 mm/yr) [*Altay and Sav*, 1991] was 82% of the mean slip geodetic slip rate (9.3 mm/yr) [*Deniz et al*., 1993] in approximately the same time interval, although reevaluated rates for the creep meter (7.3 ± 0.1 mm/yr, Figure 7a) and the geodetic data (8.7 mm/yr) [*Kutoglu and Akcin*, 2006] permit a range of 78–87%. Distributed shear tens of meters from a primary fault trace is common on creeping faults and is occasionally related to slip on contiguous traces [*Bilham and Whitehead*, 1997; *Galehouse and Lienkaemper*, 2003; *Çakir et al*., 2012; *Lindsey et al*., 2014]. Hence, the amplitude of the continuous creep meter data should be multiplied by 1.2–1.4 to correct for this incomplete sampling of the shear zone. The rates from recent creep data must be increased by a factor of ≈ 1.25 for it to agree with the recent geodesy; however, the geodetic estimates average rates obtained from somewhat different along-strike segments of the fault. This amplification factor applies both to long-term creep rates and to the amplitude of recorded creep events measured by the creep meter. To prevent confusion, and because the scaling factor is currently an approximation, this scaling factor is omitted in the discussion of creep event amplitudes and velocities in the following section except where specified.

4. Creep Events

Due to the currently uncertain amplitude-scaling factor of the creep events caused by the creep meters' incomplete span of the Ismetpasa shear zone, we leave to a future study the determination of the rate- and state-dependent properties of the fault zone and here examine the evolution of surface slip during the creep events of 1987 and 2015. Although the measured amplitudes of the creep events differ in the two creep meter installations due to their different lengths, the evolution of slip with time in each creep event should be unaffected. In what follows we analyze the observed data without correction for these unknown amplitude errors. Thus, estimates for displacement, strain, and velocity mentioned in this following section underestimate their true values by 1.2–1.3.

Table 2. Creep Event Amplitudes and Velocities, With Parameters Fit to a Double Exponential (1) for the Interval 0.5 to 30 h Following the Start of Each Creep Event[a]

Event	Slip (mm)	V_{max} (mm/h)	A	$-A_1$ (mm)	±	τ_1 (h)	±	$-A_2$ (mm)	±	τ_2 (h)	±	χ^2
8 May 1987	1.8	3.54	1.77	0.62	0.07	1.8	0.3	0.47	0.05	14.6	5.6	0.003
1 Jun 1987	2.5	1.57	2.31	0.96	0.04	1.1	0.1	0.77	0.02	11.4	1.3	0.009
17 Apr 2015	2.4	0.54	2.29	1.59	0.06	2.4	0.1	0.8	0.1	24.3	9.2	0.03
24 Apr 2015	1.9	0.40	1.52	0.76	0.18	2.1	0.3	0.5	0.2	6.3	1.7	0.006
10 Dec 2015	1.3	0.36	1.39	0.81	0.01	2.9	0.07	0.53	0.01	37.5	0.94	0.03
15 Dec 2015	1.3	0.18	0.94	0.56	0.02	3.3	0.01	0.34	0.05	15.5	0.01	0.007

[a]Slip in column 2 is estimated from data shown in Figures 7 and 9. The values for displacement and velocity shown in Tables 2–4 should be multiplied by 1.2–1.4 to account for incomplete sampling of the fault zone.

The six creep events available for analyses resemble each other in general appearance and presumably represent a small patch, or several patches, of the fault slipping aseismically with neither rigorous time-predictable nor slip-predictable behavior. In the 8 years of instrumental data reproduced by *Altay and Sav* [1991], slip events on the fault occur within clearly defined limits; slip on the fault apparently never lags more than 6 mm behind the mean creep rate and never overshoots this mean rate by more than 4 mm. Our current data, which conform to a narrower ±2 mm band (Figure 9), thus may be atypical of the longer-term creep behavior of the fault. To illustrate this apparent difference, we have superimposed our recent creep data on a part of the 1982–1990 creep data it most resembles (Figure 7a). The similarity between the 1988/1989 and 2014/2015 data emphasizes that sequences of cumulative creep events, with large amplitudes, are separated by longer periods of quiescence than we have recently recorded.

The 10 mm range of displacements evident between the slip limits shown in Figure 7a can be used to deduce approximate maximum strains in the uppermost 5 km of the fault zone. They correspond to maximum shear strains of 2×10^{-6} if strain accumulation and release is confined to one side of the fault only or as is more likely, antisymmetric shear strain of 10^{-6} on each flank of the fault (≈5 mm in 5 km). In contrast, our current data lag or lead the past 2 years' mean creep rate by only 2 mm (Figure 9), which implies an antisymmetric strain storage and release budget of 2×10^{-7} on each flank of the fault. The largest discrete creep events (2.5 mm) on the fault are associated with strain release of 2.5×10^{-7} strain.

The maximum slip velocity we recorded in 2015 was 0.54 mm/h, but the maximum recorded by Altay and Sav in May 1987 was 3.54 mm/h (Table 2). This large difference is not due to the different spatial sampling widths of the two creep meters but to the difference in the temporal sampling rate. Our telemetered 30 min sampling interval underestimates maximum fault slip velocities, because these velocities have short duration and are manifest in the first several minutes of each creep event only. The 1980 strip chart data sampling once every 12 s captured these fast initial slip rates. The duration of each creep event exceeds several hundred hours, but most of the slip occurs in the first 5 h.

We first compare the creep events recorded in 1987 with those recorded in 2015 using a double exponential decay curve of the form:

$$\mathrm{slip}(t) = A_0 + A_1 e^{-(t/\tau_1)} + A_2 e^{-(t/\tau_2)} \mathrm{mm} \quad (1)$$

where t is the time after the start of the event. The parameters in this expression describe the amplitude and decay of the creep event but have no physical significance. They can be fit to the data quite precisely (misfits are $< \pm 50$ μm), permitting a simple comparison of creep event characteristics separated by three decades (Table 2). The 1987 data were first corrected for their nonlinear chart scale using a *Rustrak* pen radius of 62 mm (F. Wyatt, personal communication). To avoid biasing the comparisons by using data of different durations, we truncated all the data to the same 0.5–30 h window before solving for the parameters in (1). Each creep event can be characterized by a rapidly decaying signal with decay rate $1 < \tau 1 < 3.3$ h, followed by a longer-period decaying process with decay rate $6 < \tau 2 < 37$ h.

Although τ_2 averages 19 ± 11 h for creep events considered in 1987 and 2015, the initial time constant, τ_1, for the 1987 data is approximately half that for the 2015 data. We note that the 1987 creep events constitute the largest cumulative sequence of events observed by *Altay and Sav* [1991] in 8 years of recording and therefore may have been anomalous. The sequence started 8 May, followed by minor events on 24 and 28 May with

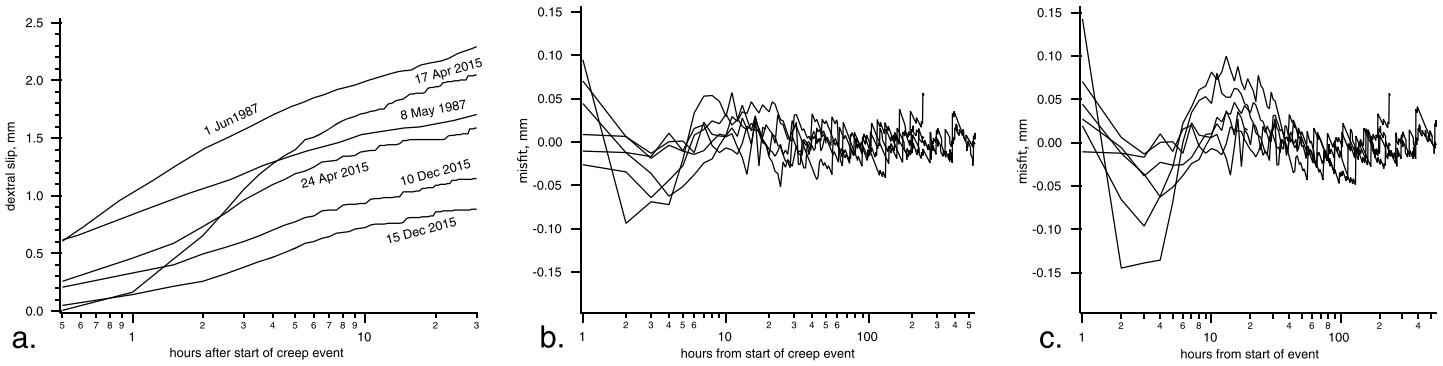

Figure 11. (a) Log linear plots of creep events from 1987 and 2015. Misfits to (b) double exponential equation (1) and (c) a three-parameter physical description of surface slip (equation (2)) that less precisely emulates the initial slip of each creep event. The step-like nature of the creep signal is caused by stiction in the creep meter with an amplitude of 20–30 μm.

amplitudes of 1.8 mm, 0.66 mm, and 0.68 mm, respectively (written by hand on the charts digitized in Figure 7 b) bringing the total slip in May (excluding slow slip between these events) to 3.05 mm. For June they summarize total monthly slip as 8.4 mm in their text, only 2.54 mm of which is accounted for in the 1 June creep event. This 1 June event was associated with the most rapid initial slip, the shortest time constant, and the largest amplitude, causing the record to go off scale. An additional 5.86 mm of creep (two to three missing creep events) thus occurred in June, which these authors either recorded as micrometer offsets or chose not to reproduce in their article.

We next fit the creep event data to an expression for a static (nonpropagating) creep event proposed by *Wesson* [1988].

$$u(t) \;=\; u_{\max}\left\{1 - \left[Ct(b\text{-}1)\; u_{\max}{}^{(b\text{-}1)} + \Delta t + 1\right]^{-1/(b\text{-}1)}\right\} \tag{2}$$

Where $u(t)$ is the slip on the fault at time t (for $b > 1$) and we introduce Δt to adjust for the data sampling interval to account for the unknown initiation time of the creep event relative to the internal clock in the data logger. The solution includes the final amplitude $u_{\max} = \sigma\, d_e / \alpha\mu$ (mm) of the creep event, and a rheological parameter $C = [(\alpha\mu / d_e)^b/k]$ mm$^{(1-b)}$/s, where σ is the shear stress applied to the fault, d_e is the depth of slip, α is determined by the aspect ratio of the fault slip event ($\alpha = 0.61$ if the total length of the slipping zone is d_e; $\alpha = 0.5$ if the slipping zone is infinitely long), and $\mu \approx 30$ GPa. For a viscous fault $b = 1$ and $k = \eta$/W, the ratio of the viscosity of the fault zone to its width.

The slip histories of the six events can be approximately fit to equation (2) (misfits are shown in Figure 11c) yielding an average value for the exponent $b = 2.7$ ($1.3 < b < 4.5$) confirming that simple viscosity is inappropriate. This average value is twice that derived by *Wesson* [1988] for the northern segment of the creeping zone of the San Andreas Fault in central California. The solutions for C, $u_{\max}$, and b are listed in Table 3. The shear stress at failure, $\sigma = \alpha\mu u_{\max} / d_e$, is determined by the geometry of the slipping zone and by the strain released by the slipping patch. If we adopt the shallowest inferred depth of the creeping zone as $d_e = 5$ km, we derive an average value of $\sigma = 0.009 \pm 0.002$ MPa, consistent with the low strain release (10^{-6}) inferred from depth and slip amplitude above. From the mean value of C and b we derive a mean value for k of 3.5×10^{-12} kg m^{-2}s^{-1}.

An improved fit to the data (±20 μm) can be obtained from equation (3) which assumes that the two depths for quasi steady slip ($u_{\text{slow}} \leq 1$ km) and event-like slip ($u_{\text{event}} \leq 5$ km) are associated with equations of similar form but different slip parameters:

$$\mathrm{u(t)} \;=\; u\left\{1 - \left[Ct\;(b_0\text{-}1)\;u^{(b0\text{-}1)} + 1\right]^{-1/(b0\text{-}1)}\right\} + u/5\left\{1 - \left[C_1 t\;(_{b1\text{-}1})\;(u/5)^{(b1\text{-}1)} + \Delta t + 1\right]^{-1/(b1\text{-}1)}\right\} \tag{3}$$

In practice, the final amplitude, $u = u_{\max}$ in equation (3) for the 2015 creep events can be fixed by inspection (e.g., from Figure 9) leaving five unknowns (Table 4). The misfits resemble those shown in Figure 11b, i.e., they do not show the systematic misfit characterized by Figure 11c. As anticipated, the rheological parameter b_1

Table 3. Creep Event Parameters Derived for Equation (2) With Their Uncertainties[a]

Event	u (mm)	$\pm u$	C	$\pm C$	b	$\pm b$	$-\Delta t$	$\pm\Delta t$	χ^2
8 May 1987	1.91	0.07	0.29	0.05	2.7	0.4	0.24	0.07	0.005
1 Jun 1987	2.80	0.75	0.064	0.02	3.8	0.25	0.68	0.15	0.004
17 Apr 2015	2.14	0.1	0.19	0.01	1.7	0.1	0.16	0.03	0.060
24 Apr 2015	1.52	0.01	0.33	0.01	1.3	0.1	0.0	0.05	0.006
10 Dec 2015	1.3	0.05	0.23	0.02	2.2	0.5	0.03	0.02	0.008
15 Dec 2015	1.52	0.17	0.052	0.68	4.5	0.01	0.45	0.01	0.019

[a]The curves systematically misfit the rise time and early slip in the data (see Figure 11c) resulting in large uncertainties in some of the C solutions. Δt (s) is an offset caused by the data logger sampling interval.

for the second term in equation (3) is smaller in each case than the first term b_0 that describes the onset of each creep event ($b_1/b_0 \approx 0.6$). For the 1987 events the value of the b_1 parameter is close to that describing purely viscous slip.

5. Afterslip

In the preceding sections we presented evidence for aseismic offset of the fault since 1957 in the form of repeated measurements of alignment arrays, steady offset of the Ismetpasa stone wall, and in the form of two multiyear segments of continuous creep monitoring. In this section we extend the fault slip record to the time of the 1944 earthquake (05:22 local time, 1 February 1944), first by extrapolating the apparent slowing in rate 1957–2016 to the time before construction of the Ismetpasa wall and then by invoking additional estimates of slip reported as coseismic slip in 1944 and as inferred afterslip in 1950.

Seven years prior to wall construction, in 1950, the nearby 1934 railroad track was reported to have been offset by 30 cm (*Ambraseys*, 1970), a value that lacks both an estimate of uncertainty and, as we discuss later, an indication of whether or not a correction for fault obliquity has been applied. We later discuss the implications of correcting this and the coseismic slip value stated by *Ambraseys* [1970] to dextral slip, but we first adopt this hitherto accepted afterslip value of 30 cm to demonstrate fits to possible time-dependent decay rates. Using an exponential expression for the decay in afterslip displacement with time

$$\text{afterslip} = k + Ae^{-t/\tau} \tag{4}$$

where k is a linear interseismic velocity and A is the amplitude of transient afterslip decaying at a rate of t/τ at time t following the main shock; the best fit in a least squares sense solving for incremental displacements in the periods 1944–1950, 1957–1969, and 1969–2016 yields $A = 40$ mm, $k = 9.8$ mm, and $\tau = 10$ years. If we assume this characterizes the entire interseismic cycle, cumulative estimated interseismic surface slip will amount to 2.4 m, assuming an earthquake recurrence interval of ≈ 200 years (Figure 5c).

We also fit the data to AFTER (equation (5)), an afterslip decay curve that has been invoked to describe slip on California strike-slip faults that slip both seismically and aseismically [*Boatwright et al.*, 1989, *Lienkaemper et al.*, 2016].

$$\text{afterslip} = u_f \left(\frac{t/T}{t/T + 1} \right)^c \tag{5}$$

The empirical expression invoked by AFTER includes a final slip term, u_f, that represents the sum of coseismic and total afterslip displacement that we initially set to 4.4 m [*Kondo et al.*, 2005], a characteristic exponent, c,

Table 4. Parameter Fits to Equation (3) Assuming That Slow Slip Processes Shallower Than 1 km Are Active During a Deep Creep Event Extending to >3 km Depth

Event	u (mm)	C_0	$\pm C_0$	C_1	$\pm C_1$	b_0	$\pm b_0$	b_1	$\pm b_1$	$-\Delta t$	$\pm\Delta t$
8 May 1987	1.6	0.33	0.48	0.01	0.23	1.6	0.7	1.01	0.02	0.01	0.01
1 Jun 1987	2.54	0.29	0.01	0.003	0.001	2.7	0.05	1.02	0.9	0.001	1.4
17 Apr 2015	2.3	0.23	0.01	0.019	0.001	1.59	0.04	1.3	0.2	0.33	0.01
24 Apr 2015	2.1	0.069	0.006	0.006	0.002	3.67	0.07	2.1	0.3	0.09	0.06
10 Dec 2015	1.3	0.258	0.009	0.156	0.005	2.54	0.05	1.36	0.01	0.01	0.01
15 Dec 2015	1.3	0.248	0.009	0.016	0.005	2.54	0.05	1.36	0.18	0.01	0.01

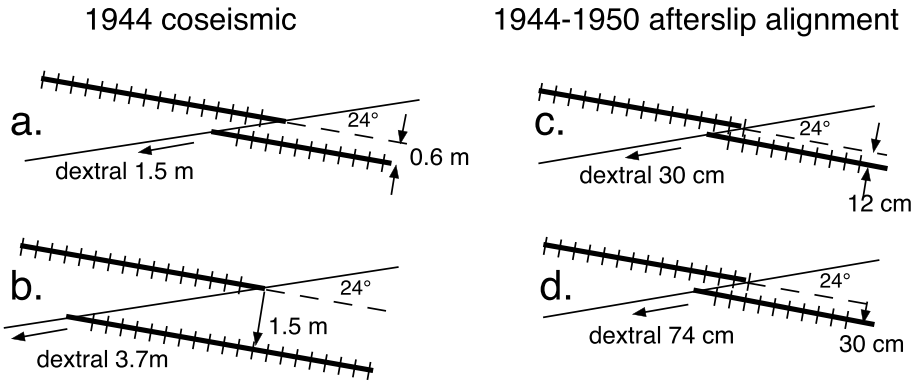

Figure 12. Alternative interpretations for rail offset and dextral fault slip. Railroad line offsets were considered to describe (a and c) dextral offsets by *Ambraseys* [1970] and by subsequent authors. However, if the railroad engineers were describing offsets in the alignment of the rails, the implied dextral fault slip is increased by a factor of 1/sin24°. The (b) cumulative coseismic slip (3.7 m) and (d) afterslip (0.74 m) is consistent with the 3.6–6 m of slip documented by Kondo *et al.* [2015] nearby for the 1944 earthquake.

that determines the decay rate and a variable $1/T$, where T is the effective duration of the afterslip process. In solutions that fit the observed wall offset data we determined $0.8 < c < 0.9$ and $100 < T < 550$ days. However, all solutions required pre-1950 slip to have been less than 115 mm. If we ignore this apparent misfit, we would conclude that for a 6 m seismic cycle (releasing ≈ 276 years of interseismic plate motion), afterslip in the interseismic interval amounts to ≈ 1.4 m followed (and preceded) by coseismic slip of 5.6 m (Figure 3c). In Figure 12 we illustrate graphically that the pre-1957 reports of offset at Ismetpasa may have been misinterpreted, which would render the above values for interseismic slip extrapolated from the 1957–1969 data considerably in error.

The railroad lines at Ismetpasa are stated to have been offset coseismically by 1.5 m in the 1944 earthquake [*Ambraseys*, 1970]. We here question whether this stated number represents dextral slip or their lateral offset from a former straight line (Figure 12). Ambraseys' statement "displaced the Zonguldak railroad line by about 150 cm" has been construed to quantify dextral slip [*Kondo et al.*, 2005], and Ambraseys certainly implied this in the context of his article. However, the 1.5 m of observed offset is significantly lower than the 3.6 m–6 m offsets *Kondo et al.* [2005] measure in the form of offset rows of trees, irrigation canals, dirt roads, and field boundaries 1 km to the west and 2.5 km to the east of the railroad (Figure 13b). If we suppose that the reported railroad offset of ≈ 1.5 m were not of dextral slip (Figure 12a), but a report of misalignment of the railroad lines following their repair (Figure 12b), the dextral offset must be increased by 1/sin24° to ≈ 3.7 m.

Likewise, the interpretation of the second adjustment to the rails in 1950, following the initial 1.5 m realignment in 1944 requires reevaluation. Here *Ambraseys* [1970] states that in 1950 "the railroad tracks were again distorted at the same point showing a displacement of 30 cm." A buckle in the rails had developed that required trains to slow as they approached Ismetpasa station from the west. To correct a quite minor rail-normal misalignment of ≈ 12 cm the railroad, engineers would have needed to shorten the rails by removing a 32 cm length of steel track (Figure 12c). Alternatively, if there were truly a misalignment of the line of 30 cm (Figure 12d), it would have required the dextral fault afterslip accumulated since 1944 to have been 74 cm.

Thus, it appears to us very probable that the 1944 earthquake resulted in 3.7 m of dextral slip when the railroad tracks were repaired and an additional 0.74 m of afterslip by 1950. We admit the possibility that the numbers recorded by *Ambraseys* [1970] may have been rounded to decimeters suggesting that no great accuracy should be ascribed to them. If we assign ±20 cm to the 1.5 m 1944 estimate and ±10 cm to the 30 cm misalignment in 1950, the combined fault slip and its uncertainty 1944–1950 becomes 4.4 ± 0.7 m (Table 5).

Treating the precise time of the initial 3.7 m of inferred dextral offset as a variable and using the constraints in rows 1, 2, 4, and 5 of Table 5 in equation (5), we solve for the time of the initial repair to the railroad. The railroad was constructed a decade before the 1944 earthquake; however, we ignore 1934–1944 late interseismic slip on the fault which would reduce coseismic slip by approximately 6 cm were it similar to current rates, an amount that is embraced by the ±20 cm uncertainty estimated for the coseismic slip. We calculate that the

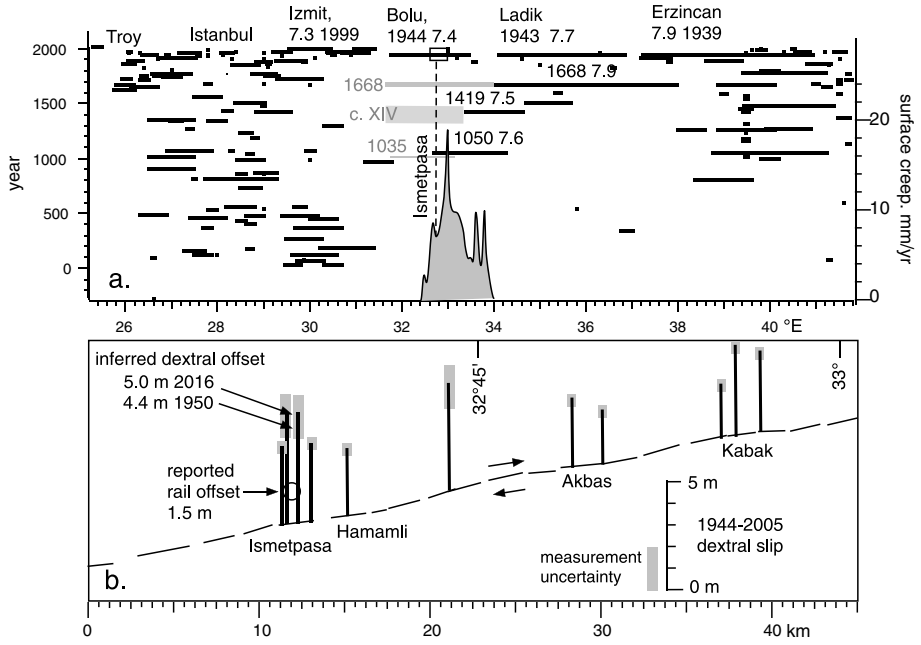

Figure 13. (a) Earthquake rupture space-time diagram along the North Anatolian fault for the past 2000 years [*Bohnhoff et al*., 2016] including inferred earthquakes (grey bars) near Ismetpasa in the Bolu/Gerede segment from *Kondo et al*. [2010]. Surface creep [*Cetin et al*., 2014] is shaded grey, and the rectangular box on the Bolu/Gerede earthquake rupture is enlarged in the lower panel. (b) Map view of Ismetpasa segment showing field offsets from *Kondo et al*. [2005] compared to reported rail offset (circle) from *Ambraseys* [1970]. The rail offset is much lower than neighboring offsets but is close to the 4.4 m dextral slip (arrowed) 1950 offset calculated at Ismetpasa assuming that the rails cross the fault obliquely at 24°. Nearby field offsets are indistinguishable from the ≈ 5 m of cumulative slip including post 1950 afterslip.

reported "1.5 m railroad offset" corresponds to the second day after the earthquake, a plausible time for engineering repairs to the railroad.

The values in Table 5 potentially permit afterslip to be distinguished from the presence of steady creep on the fault. The accuracy with which this can be achieved depends on several assumptions, including the precise timing of the initial railroad repair, that constrain the 1944–1950 afterslip interval. We consider it probable that the 3.7 m deduced to have distorted the rail line at Ismetpasa would not have been manifest within seconds of rupture as coseismic slip but instead was manifest entirely as afterslip reaching the surface starting minutes or hours after the main shock. This appears to us plausible because surface slip has been delayed

Table 5. Coseismic Slip, Afterslip, Wall Offset, and Estimated Uncertainties at Ismetpasa[a]

		Offset		Dextral		
Row	Epoch	Published (m)	Process	Slip (mm)	Uncertainty (mm)	Time Interval (year)
1	1 Feb 1944	1.5[b]	coseismic	3700	490	0 to 30 days
2	1944–1950	0.3[b]	afterslip	740	25	20 days to 6 years
3	*1950–1957*	*none*[b]	*data gap*	*≈114*	*≈15*	*6 to 13 years*
4	1957–1969	wall photos	wall offset	125.4	10	13-25 years
5	1969–2016	wall photos	wall offset	516	15	13 to 72 years
6	**1944–2016**	**3.6-5 ± 1**[c]	**cumulative slip**	**4990**	**555**	zero to 72 years
7	*1668–1944*	*6.072*	*slip potential*	-	*276*	*276 years*
8	*2016–2220*	-	*interseismic residual*	*1081*	*380*	*204 years*

[a]Column 5 assumes published values refer to rail offsets and are corrected by 1/sin24° to convert to dextral slip. We calculate fault slip in the interval 1950–1957 as 114 mm using the stated 1944, 1950, 1969, and 2016 offsets (see text). The interseismic residual is the difference between the slip potential (276 years at 22 ± 1 mm/yr) and the current surface slip (2016) assuming a similar interseismic renewal time. Bold text (row 6) indicates calculated surface slip to 2016. Rows 7 and 8 indicate inferred interseismic slip and current residual. Rows in italics are estimated or calculated rather than observed.
[b]Stated by *Ambraseys* [1970].
[c]Reported by *Kondo et al*. [2005]. The slip potential estimate assumes a plate velocity of 22 ± 1 mm/yr.

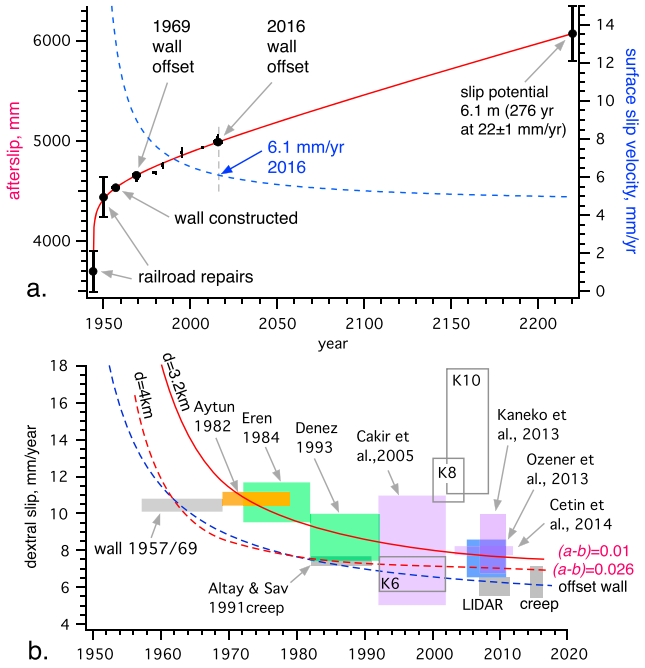

Figure 14. (a) Railroad and wall offsets (from Table 5) as a function of time. The best fit red line to the displacement data is obtained by simultaneously solving for a linear creep velocity (4.65 mm/yr) and afterslip predicted from equation (2). (b) Compilation of observed fault slip velocities from Table 6 (K6, K8, and K10 are identified in Table 5 and discussed in the text). While continuous creep measurements and LIDAR [*Karabacak et al.*, 2011] generally agree with velocities derived from wall offsets (grey boxes and blue dashed line from Figure 14a), most geodetic estimates indicate an ≈ 1.25 faster velocity as depicted by the solid red line (predicted velocity decay curve for $(a\text{-}b) = 0.01$ and locking depth of 3.2 km from *Kaneko et al.* [2013]). The red dashed line corresponds to their calculation for locking depth of 4 km and $(a\text{-}b) = 0.026$. Measurements with narrow aperture indicate a present-day (2016) creep rate of 6.1 mm/yr, whereas large-scale measurements (orange, 155 m alignment array; green and blue, ≈ 800 m GPS array; and violet, >30 km InSAR) favor a rate closer to 7.6 mm/yr. Some of the geodetic measurements include velocity estimates from regions to the east where slip rates are higher.

in several Anatolian earthquakes by many hours. For example, *Ambraseys* [1970] recounts that in the 22 July 1967 Mudurnu earthquake at Acemler, paths were offset and an irrigation ditch flooded the village many hours after rupture. Examples of delayed surface slip are common on creeping faults in California. No surface occurred coseismically for 5 h on the *M*6.8 1987 Superstition Hills earthquake [*Bilham*, 1989] nor on the southern segment of the *M*6.0 2004 Parkfield rupture for 3 days [*Bilham*, 2005; *Langbein*, 2006] nor in the Napa earthquake [*Lienkaemper et al.*, 2012] in California. Thus, we suppose that in 1944 the "coseismic" slip and afterslip constitute different stages of an evolving afterslip process that may have been largely completed by 1950 and which now contributes <25% to the observed aseismic slip rate at Ismetpasa.

The rapid decay in afterslip prior to 1957 suggests that the currently observed creep on the Ismetpasa segment is now driven largely by a plate boundary stressing process similar to that occurring in central California. Accordingly, we fit the data numerically to the sum of the right-hand side of equation (2) and a linear slip term vt, where t is the time after the earthquake and v is a steady interseismic velocity constrained by the parameters listed in Table 5 to be 4.65 mm/yr. Residual afterslip plus this background velocity yields a current (2016) slip rate of 6.1 mm/yr (Figure 14a) and suggests that an additional slip of ≈ 1 m will accumulate before the next earthquake supposing that the next Bolu-Gerede earthquake recurs in ≈ 2220 CE. *Ambraseys* [1970] reports no rail realignments in the period 1950–1969 during which time we estimate 24 cm of dextral slip, corresponding to 9.8 cm of rail misalignment (Figure 14a). The 1951 earthquake [*Eyidogan et al.*, 1991] does not appear to have contributed significantly to surface slip despite mention of surface cracks [*Ambraseys*, 1970] and minor buckling of the rails [*Ketin*, 1957; *Aytun*, 1982]. Slip during the 1950–1957 interval (before wall construction) is calculated to have been 114 mm corresponding to a mean slip velocity of 16 mm/yr, slowing to 10.4 mm/yr between 1957 and 1969, and 8.7 mm/yr between 1969 and 2016, consistent with rates calculated from the offset wall. Adopting the lower or higher range of uncertainties for the railroad offsets increases the misfit significantly and shifts the estimated time of the first railroad measurement but does not change the interseismic background velocity. No solution was possible for a calculation using the raw-railroad offsets (1.5 m in 1944 and 0.3 m in 1950) as input.

6. Discussion

The 150 km length of the creeping zone on the North Anatolian Fault [*Cetin et al.*, 2014, Figure 13a] is comparable to that of the creeping central San Andreas fault; however, earthquakes that have ruptured the ends

Table 6. Ismetpasa Slip Velocities From Wall Offsets, Creep Meters, LIDAR, Triangulation, Trilateration, GPS, and InSAR[a]

Source	Published (mm/yr)	Method	Interval	Duration (year)	Aperture (m)	Adopted (mm/yr)	1σ (mm/yr)
Ambraseys [1970]	20	photo	1957–1969	12	47 m	10.4	0.4
Aytun [1982]	15	photo	1957–1969	12	47 m	10.45	0.35
Aytun [1982]	10	triangulation	1969–1979	10	160 m	10.8	0.4
Eren [1984]	≈10	trilateration	1072–1982	10	800 m	10.2 (10.6)	0.6 (1.1)
Deniz et al. [1993]	9.6	trilateration	1982–1992	10	800 m	9.3 (8.7)	0.7 (1.3)
K6—*Kutoglu and Akcin* [2006]	7.8	GPS	1992–2002	10	800 m	7.8 (6.7)	0.5 (1.1)
Altay and Sav [1991]	7.6 ± 0.1	creep meter	1982–1991	9	15 m	7.3	0.1
K8—*Kutoglu et al.* [2008]	12 ± 1.3	GPS	2002–2007	5	800 m	12.0	1.3
K10—*Kutoglu et al.* [2010]		GPS	2002–2008	6	800 m	15.1	4.1
Çakir et al. [2005]	8 ± 3	inSAR	1992–2002	10	>50 km	8.0	3.0
Cetin et al. [2014]	8.35 ± 0.24	InSAR	2003–2011	8	>50 km	8.35	0.24
Karabacak et al. [2011]	8.4 ± 1.6	LIDAR	2007–2009	2	20 m	8.4	1.6
Ozener et al. [2013]	7.6 ± 1	GPS	2005–2011	6	800 m	7.6	1.0
Kaneko et al. [2013]	≈9	InSAR	2007–2011	4	>50 km	6	0.5
1969–2016 wall offset[b]	from Figure 5b	photo	1969–2016	47	47 m	8.3	0.1
1984–2016 wall offset[b]	from Figure 5b	photo	1984–2016	33	47 m	7.1	0.3
1969–1984 wall offset[b]	from Figure 5b	photo	1969–1984	15	47 m	9.9	0.3
2014–2016 continuous[b]	from Figure 9	creep meter	2014–2016	2	8 m	5.9	0.1
2014–2016 afterslip fit[b]	from Figure 14a	offset wall	2014–2016	2	47 m	6.1	1.0

[a]Numbers in parenthesis in the last two columns refer to a revised analysis of *Eren* [1984] and *Deniz et al.* [1993] by *Kutoglu and Akcin* [2006] (K6).
[b]Derived for stated time periods.

of the creeping zone in central California have been relatively modest (e.g., Parkfield $M \sim 6.0$), with major earthquakes ($M_w \geq 7.6$) in 1906 and 1857 abutting, rather than overlapping, those segments currently exhibiting surface creep. The combination of creep and seismic behavior of the Ismetpasa segment more closely resembles that on the Hayward fault, where apparently steady creep rates of 5–9 mm/yr are interrupted by $M_w \leq 7$ earthquakes at ≈ 160 year intervals [*Lienkaemper et al.*, 2012]. At least since 40 years after the 1868 earthquake mean creep rates at Fremont on the Hayward fault have been steady, as documented by a foundation wall that has now been offset in Fremont by ≈ 1 m. This time interval represents 80% of the earthquake cycle, but it is probable that rapid initial (but undocumented) afterslip occurred prior to wall construction in Fremont [*Lienkaemper et al.*, 2016]. The duration of observed surface creep data at Ismetpasa starting 13 years after the 1944 earthquake is currently only 26% of the inferred ≈ 276 year earthquake cycle for major earthquakes here (1944–1668), and early afterslip is evident in the numerical data. However, in contrast to previous studies at Ismetpasa, the decadal-averaged creep rate at Ismetpasa has slowed by only ≈ 12% since creep was first discovered in 1969. In the following sections we discuss the implications of the transition from coseismic slip to what appears now to be linear but episodic surface creep, on the interpretation of 1994 earthquake magnitude and on the role of creep in the interseismic cycle.

6.1. Current Creep Rates Near Ismetpasa

The velocities plotted in Figure 14b show a bimodal distribution. Those with a fault-normal aperture <20 m (wall offsets, LIDAR, and creep meter data) must be multiplied by approximately ≈ 1.25 to bring them into agreement with triangulation, GPS, and InSAR data with their considerably larger observational footprints. The correction factor is common on creeping faults where surface shear is sometimes distributed tens of meters from a discrete offset that may accommodate 75–90% of the shear displacement manifest across the surface fault [*Galehouse and Lienkaemper*, 2003]. We allude to this correction factor in our discussion of the results from creep meters, where we argue that incomplete sampling of the surface shear zone by creep meters requires observed creep event parameters to be increased in amplitude by a factor of 1.2–1.4. Some of the creep rate estimates include velocities from segments of the fault to the east where creep rates are known to be higher [e.g., *Cetin et al.*, 2014]. A further discrepancy between near-fault slip measurements and geodetic data acquired far from the fault is that in addition to the near-fault strain field caused by slip on the surface fault down to a locking depth of 5–7 km, these distant measurements increasingly sample a regional strain field with an arc-tan signature caused by creep below the seismogenic zone.

6.2. Accelerations in Slip Rate?

Apart from the episodic rate changes associated with surface creep events we find no evidence to support changes of rate on the fault related to distant seismicity. However, some authors have claimed significant changes in rate based on the apparent outliers evident in Figure 14b. These are labeled K8 [*Kutoglu et al*., 2008] and K10 [*Kutoglu et al*., 2010] that we now briefly discuss. The two time intervals with high velocities recorded are 5 and 6 years duration with velocities of 12.0 ± 1.3 and 15.1 ± 4.1, respectively, preceded by a contiguous 10 year interval with 6.7 ± 1.1 mm/yr velocity (K6), suggesting an acceleration in slip rate in the interval 1992–2008 (Table 5). This anomalous acceleration has been discussed subsequently by *Kutoglu et al*. [2012] and by *Gormus et al*. [2013]. The weighted mean velocity for these three epochs would be 8.9 ± 5 mm/yr, similar to InSAR measurements in the early part of this window (1992–2002; 8 ± 3 mm/yr) [*Çakir et al*., 2005] and GPS measurements near the end of this time window (200512011; 7.6 ± 1 mm/yr) [*Ozener*, 2013] which do not register this increase in rate. We note that short segments of geodetic data yield erratic velocities due to the influence of creep events on the fault with slip amplitudes of as large as 16–20 mm; however, such events would influence 5 year sampling interval velocity estimates by only 2 mm/yr. We therefore cannot account for reported velocities exceeding 10 mm/yr 1999–2008. The cumulative offset of the wall indicates that no unusual increment in slip occurred between 1999 and 2016, which therefore refutes any long-term contribution to cumulative slip from K8 or K10.

Cetin et al. [2014, Figure 8] document the effects on the fault of the 6 June 2000, $M_w = 6.0$ Orta earthquake, a normal faulting event that occurred ≈ 35 km SE of Ismetpasa [*Taymaz et al*., 2007; *Çakir et al*., 2005] and was accompanied by numerous aftershocks. It is possible that this earthquake may have locally shifted the control points analyzed by *Kutoglu et al*. [2008, 2010, 2013].

6.3. Magnitude of the 1 February 1944 Bolu/Gerede Earthquake?

Kondo et al. [2005] estimate the 1944 earthquake as $M_w = 7.6$, based on its 175 km long rupture and their mean observed surface slip of 3.4 m. They correctly note that their observed surface slip includes afterslip, but we argue above that *all* of the surface slip in the Ismetpasa segment may be a combination of afterslip combined with steady creep. This differs from the model presented by *Kaneko et al*. [2013], who assume 50% coseismic surface slip, 20% afterslip, and 30% interseismic creep. The distinction is important because if no coseismic surface slip occurred shallower than, say, 5 km, the moment magnitude would need to be adjusted downward by 0.2 magnitude units to $M_w = 7.4$. If velocity strengthening inhibited coseismic slip in the uppermost 7 km of the fault, the resulting magnitude would be closer to the magnitude $M_s = 7.3$ determined by *Dewey* [1976]. However, our $M_w = 7.4$ magnitude estimate may err on the low side because creep currently decays westward [*Çakir et al*., 2005], admitting the possibility that as much as two thirds of the western rupture may have been entirely coseismic from the base of the seismogenic zone to the surface. The absence of shallow present-day creep presently to the west, however, does not mean that rate and state friction moderated afterslip did not occur in the near-surface rupture of segments west of Ismetpasa following rupture.

6.4. Interseismic Creep and the Earthquake Cycle

In Figure 14a we illustrate the inferred development of 6.1 m of surface slip during the entire earthquake cycle (276 ± 40 years) based on measured slip in the past 72 years. By definition, this 6.1 m is equal to the seismogenic slip potential of the seismogenic zone at the end of the earthquake cycle. If we assume that a substantial fraction of the afterslip in the uppermost 5–7 km of the fault was largely complete by 1969, 25 years after the main shock, the implication is that at the current stage in the interseismic period (72 years after the main shock) and for the remainder of the interseismic interval, surface creep now responds largely to plate boundary stressing processes. This observation is significant because it implies that the base of the surface creeping zone is no longer responding to stress from the last major earthquake. Instead, the upper surface of the seismogenic zone that will eventually rupture in a future earthquake is now being incrementally stressed by creep events. The monitoring of creep events thus has utility in monitoring processes that may occur as a prelude to an approaching future earthquake rupture. Based on a 276 year historical recurrence time, an additional 1 m of surface creep is anticipated before the next major earthquake here (Figure 14a).

Of the 5.9 ± 0.1 mm/yr slip rate presently recorded by the Ismetpasa creep meter we calculate from equation (5) that 1.25 mm/yr (21%) may be attributable to residual afterslip and 4.65 mm/yr (79%) from linear creep driven by present-day loading. With the base of the seismogenic zone at 12 km the inferred base of this linear

creep would lie at a depth of ≈ 2.9 km, whereas the total 5.9 mm/yr creep signal would be inferred to extend to a depth of ≈ 3.6 km. The formulation thus implies that the slowing in surface creep is caused by a geometric shallowing in the depth of creep events on the fault.

In contrast, the velocity strengthening formulation investigated by *Kaneko et al*. [2013] predicts that the depth of creep should increase during the interseismic interval. In Figure 14b we compare our corrected afterslip rate curve with two models published by *Kaneko et al*. [2013] for locking depths of 3.2 km and 4 km using friction properties (*a-b*) of 0.01 and 0.026, respectively. Their curves steepen in the early part of the afterslip process to fit *Ambraseys* [1970] initially overestimated 20 mm/yr slip rate but otherwise provide a reasonable fit to our data. Their model, however, differs substantially in the first year of the earthquake during which they envisage coseismic surface rupture followed by afterslip, whereas we infer zero surface slip during the main shock and a surface slip signature that develops entirely postseismically. Clearly, it would be desirable to examine physically based afterslip models using the new early constraints supplemented by additional data from creep events.

Assuming a current creep rate of 6.1 mm to 7.6 mm year (Figure 10c), a depth-averaged shear strain is accumulating at 1.5–1.7 μstrain/yr on the uppermost 3.6 km to 5 km of the fault, corresponding to 0.75–0.85 μstrain/yr. An implication is that in the 220–276 years between major earthquakes on this segment, the antisymmetric shear strain in the uppermost 5 km of the fault prior to rupture will have incremented by 165–230 μstrain. If we exclude inferred afterslip and use instead the inferred linear creep rate of 4.65 mm/yr above 2.9 km depth, the depth-averaged strain accumulation rate is 0.8 antisymmetric μstrain/yr. The implied strain at failure is twice that anticipated on flanks of the Hayward fault (83 ± 34 μstrain) that slips for most of its length at 5 mm/yr down to a creeping depth of 5 km between major earthquakes [*Lienkaemper et al*., 2012].

The 1982–1991 creep meter data suggest that variations in surface creep rate occur with a multiyear cycle. The cause of these long-term variations may be that somewhat deeper patches of the fault occasionally slip or that pulses of slip propagate along the fault. For example, in 1987 and 1990 the surface creep accelerates following an interval of lower rates formed from slow slip and relatively modest creep events (Figure 7). Slip in 1982 may have followed such an event, and our 2014–2016 creep meter data followed a nearby ≈ 20 mm slip event on the fault [*Rousset et al*., 2016]. These 3–5 year cycles perturb the mean creep rates derived from infrequent geodetic observations. The time history of each creep event suggests that at least two decay constants are involved describing the slip process: initial slip has a characteristic decay time of 1–3 h, and subsequent slip has a time constant of 6–24 h. Individual creep events release shear strain of less than 10^{-6} on the flanks of the fault, but the shear strain released by the larger creep sequences in 1987 and 1990 (up to 16 mm in two months if we include a 1.4 scaling factor) may involve larger strain release. This depends on whether the creep events extend to greater depth during these sequences or whether they involve a propagating pulse of slip limited to uniform depth. A laterally, along-strike propagating 2 mm, surface displacement limited to 3.6 km depth would produce $\approx 0.6 \times 10^{-6}$ of flank shear strain. A larger surface creep event scaled to greater depth would involve similar strain release but would release strain over a larger volume.

Creep rates in central California are occasionally retarded or accelerated by nearby earthquakes [*Burford and Harsh*, 1980; *Schulz et al*., 1982; *Titus et al*., 2005, 2006]. We see no evidence for perturbations in the creep rate at Ismetpasa resulting from earthquakes on nearby or distant fault segments, although we concede that changes in rate may have occurred that would have escaped detection because of the absence of a continuous creep data for 42 years of the 59 year-long record. The largest slip episode recorded in May/June 1987 (12 mm observed and 16.8 mm corrected for sampling aperture) is associated with no known local earthquakes, although a 48 km distant $M_w = 4.5$ earthquake occurred 5 months prior to its onset. A yet larger creep event (≈20 mm) is inferred to have been recorded by InSAR data in 2013, 1 year before the carbon rod creep meter started recording [*Rousset et al*., 2016]. The 2013–2016 data may thus resemble the creep sequence recorded by *Altay and Sav* [1991] in 1987–1989 when a large multiple creep event was followed by minor episodes of creep in the following 2 years (Figure 7a).

7. Conclusions

Numerous previous studies of creep on the North Anatolian Fault have accepted *Ambraseys* [1970] estimate that the wall constructed at Ismetpasa in 1957 had been offset by 24 cm when he visited it with others in 1969. However, the photograph provided in his 1970 article, and those taken the same day by Aytun and

Allen and reproduced in their 1982 articles, indicates that the actual offset (≈13 cm) was considerably smaller and that its rate of offset since 1957 had been approximately 10 mm/yr, half the rate deduced from Ambraseys' original value but similar to slip rates 1969–1979. These and additional photographs and LIDAR measurements provide an absolute measure of the wall's progressive offset indicating a slowing in its rate from more than 10 mm/yr in 1969 to its current (2016) creep meter offset rate of 6.1 ± 0.2 mm/yr. Recent triangulation, trilateration, and InSAR and GPS rates that average displacements over a wider region near the fault indicate a current creep rate of 7.6 ± 1 mm/yr approximately 1.25 times faster, indicating that the creep meters and the wall sample creep from a wider shear zone than accessible to their 5–12 m fault-normal apertures.

In contrast to the stable long-term decadal creep rate, measurements with creep meters show that interannual surface slip is episodic and consists of periods of no slip (47% of the time in the past 2 years), interrupted by months of slow slip (44% of the time in the past 2 years) at rates of ≈ 3 mm/yr or by abrupt slip events with transient velocities exceeding 3 mm/h, slip durations of many days, and, in the case of multiple events, with cumulative amplitudes of many millimeters. To correct for the incomplete spatial sampling of the surface shear zone by the creep meters, their recorded displacements and velocities must be multiplied by a factor of 1.2–1.4. If we include this correction factor, the largest sequence of creep events (recorded in May/June 1978) cumulatively accounts for 16.8 mm of slip on the fault, similar in amplitude to a creep episode reported to have occurred to the east of Ismetpasa in 2013 [*Rousset et al*., 2016].

Because creep events occur at several month intervals on the fault, all measurements of surface fault slip suffer from temporal aliasing errors in estimating long-term creep rates. Typically, Ismetpasa creep events occur in pairs with cumulative amplitudes of ≈ 4 mm (≈5 mm when corrected for incomplete fault zone sampling), hence if they occurred regularly in time would occur approximately yearly. In practice, they occur erratically with no slip in some years followed by multiple sequences of events every 3–5 years. Hence, all methods require at least a decade of data if they are to yield estimates of average slip rate accurate to 10%. We see no perturbation to the long-term slowing in creep rate despite several nearby earthquakes. Recent earthquakes may have triggered minor slip when the creep meters were not operating, but this has resulted in no obvious perturbation to the apparently slow decrease in decadal surface creep rates.

The observed offset rate of the Ismetpasa wall when combined with the remotely observed shear strain rate indicates that creep initially extended to 5–7 km depth, less than half way to the base of the seismogenic zone, but that it now extends to 3.6 km, less than one third to the depth of the base of the seismogenic zone. Episodes of slow uneventful slip on the fault account for approximately 25% of the total slip but occur for 44% of the time, and we conclude that this slow slip process is confined to depths shallower than 1.8 km. From the inferred superposition of shallow slow slip during abrupt creep events at deeper depth we surmise that the rheological control of these slower processes is closer to that expected from viscous materials. Observed creep events are associated with strain accumulation and release of the order of 10^{-6} and with onset velocities $>$3 mm/h and with decay time constants of the order of 1–3 h. The largest discrete creep events, when corrected for limited fault zone sampling, exceed 3.4 mm and are often followed a few days or weeks later by a similar-sized creep event. Although these double events are likely to signify propagating creep along the fault, with data from one isolated creep meter, it is not possible to distinguish between spontaneous slip of a discrete patch and longitudinal creep propagation.

If *Ambraseys* [1970] reported offsets to the railroad in 1944 and 1950 that were statements of rail misalignment, their correction for fault obliquity requires 4.4 m of slip on the fault in the 6 years following the earthquake. With the addition of subsequent surface creep reported in this article, the resulting ≈ 5.0 m of surface slip accords with measured 1944 offsets on contiguous segments of the fault by *Kondo et al*. [2005]. We conjecture, based on an empirical afterslip decay rate, that 1944 surface slip occurred entirely as afterslip starting hours after the main shock and that residual afterslip at Ismetpasa (currently 1–2 mm/yr) is imposed on a linear background creep of ≈ 4.65 mm/yr. A further ≈ 1 m of surface slip is anticipated before the next major earthquake on the fault assuming an interseismic cycle similar to the 1668–1944 cycle [*Bohnhoff et al*., 2016] releasing an ≈ 6 m of plate boundary slip deficit. The inferred absence of surface slip in the M_s = 7.3 1944 main shock has the effect of reducing the geometric moment magnitude derived from its mean slip and surface rupture length from M_w = 7.6 to perhaps as low as M_w = 7.4. Of importance to seismic hazard

studies is the observation that creep processes are currently responding to loading caused by plate motion and that episodic surface creep events incrementally increase shear strain near the upper surface of the seismogenic zone that will eventually fail in a future major earthquake.

Acknowledgments
The project was funded by NSF grants EAR 1349851/1622720 and by Scientific Research Projects of Bogazici University under grant 10240. We thank Clarence Allen, James Jackson, and Wayne Thatcher for providing us with their original photographs of the wall at Ismetpasa and Frank Wyatt for providing us with a measure of the pen length in the *Rustrak* recorders with which we corrected nonlinearity in the 1987 chart records. The manuscript has been substantially improved following thoughtful reviews by Jim Lienkaemper, Sylvain Barbot, the Associate Editor, and an anonymous reviewer. We acknowledge the importance of independent evaluation of the Ismetpasa data, and the supporting information provide copies of the photographs used in our analysis and digital listings of the 1982–1991 and 2014–2016 creep meter data.

References

Allen, C. R. (1982), Comparisons between the North Anatolian Fault of Turkey and the San Andreas Fault of California in, *Multidisciplinary Approach to Earthquake Prediction Volume 2 of the series Progress in Earthquake Prediction Research*, edited by A. M. Isikara, et al., 67–85, iedr. Veiweg & Sohn, Braunschweig, doi:10.1007/978-3-663-14015-3_5.

Altay, C., and H. Sav (1991), Continuous creep measurement along the North Anatolian Fault zone, *Bull. Geol. Congress Turkey*, *6*, 77–84.

Ambraseys, N. N. (1970), Some characteristic features of the Anatolian Fault zone, *Tectonophysics*, *9*, 143–165.

Ayhan, M. E., and A. Kocyigit (2010), Displacements and kinematics of the Feb 1 1944 Gerede earthquake (North Anatolian fault system, Turkey): Geodetic and Geological constraints, *Turkish J. Earth Sci.*, *19*, 285–311.

Aytun, A. (1982), Creep measurements in the Ismetpasa region of the North Anatolian fault zone, in *Proceedings, Multidisplinary Approach to Earthquake Prediction*, edited by A. M. Isikara and A. Vogel, pp. 279–292, Friedr. Vieweg and Sohn, Braunshweig/Wiesbaden.

Barka, A. (1996), Slip distribution along the North Anatolian Fault associated with the large earthquakes of the period 1939 to 1967, *Bull. Seismol. Soc. Amer.*, *86*, 1238–1254.

Bilham, R. (1989), Surface slip subsequent to the 24 November 1987 Superstition Hills, earthquake, California, monitored by digital creep-meters, *Bull. Seismol. Soc. Amer.*, *79*(2), 425–450.

Bilham, R. (2005), Co-seismic strain and the transition to surface afterslip recorded by creep-meters near the 2004 Parkfield epicenter, *Seismol. Res. Lett.*, *76*, 49–57.

Bilham, R., and J. Behr (1992), A two-depth model for aseismic slip on the Superstition Hills fault, California, *Bull. Seism. Soc. Amer.*, *82*, 1223–1235.

Bilham, R., and S. Whitehead (1997), Subsurface creep on the Hayward Fault, Fremont California, *Geophys. Res. Lett.*, *24*, 1307–1310, doi:10.1029/97GL01244.

Bohnhoff, M., P. Martinez-Garzon, F. Bulut, E. Stierle, and Y. Ben Zion (2016), Maximum earthquake magnitudes along different sections of the North Anatolian Fault zone, *Tectonophysics*, *674*, 147–165.

Burford, R. O., and P. W. Harsh (1980), Slip on the San Andreas fault in central California from alignment array surveys, *Bull. Seismol. Soc. Amer.*, *70*, 1233–12,161.

Çakir, Z., J.-B. de Chabalier, R. Armijo, B. Meyer, A. Barka, and G. Peltzer (2003), Coseismic and early postseismic slip associated with the 1999 Izmit earthquake (Turkey), from SAR interferometry and tectonic field observations, *Geophys. J. Int.*, *155*, 93–110.

Çakir, Z., A. M. Akoglu, S. Belabbes, S. Ergintav, and M. Meghraoui (2005), Creeping along the Ismetpasa section of the North Anatolian fault (western Turkey): Rate and extent from InSAR, *Earth Planet. Sci. Lett.*, *238*, 225–234.

Çakir, Z., S. Ergintav, H. Ozener, U. Dogan, A. Akoglu, M. Meghraoui, and R. Reilinger (2012), Onset of aseismic creep on major strike slip faults, *Geology*, *40*(12), 1115–1118.

Cetin, E., Z. Çakir, M. Meghraoui, S. Ergintav, and A. M. Akoglu (2014), Extent and distribution of aseismic slip on the Ismetpasa segment of the North Anatolian Fault (Turkey) from persistent scatter InSAR, *Geochem. Geophys. Geosyst.*, *15*, 2883–2894, doi:10.1002/2014GC005307.

Deniz, R., A. Aksoy, D. Yalin, H. Seeger, P. Franke, O. Hirsch, and P. Bautsch (1993), Determination of crustal movement, *J. Geodyn.*, *18*, 13–22.

Dewey, J. (1976), Seismicity of northern Turkey, *Bull. Seismol. Soc. Amer.*, *66*, 843–868.

Du, W., L. R. Sykes, B. E. Shaw, and C. H. Scholz (2003), Triggered aseismic fault slip from nearby earthquakes, static or dynamic effect?, *J. Geophys. Res.*, *108*(B2), 2131, doi:10.1029/2002JB002008.

Eren, K. (1984), Strain analysis along the North Anatolian fault by using geodetic surveys, *Bull. Geod.*, *58*, 137–149.

Ergintav, S., S. McClusky, E. H. Hearn, R. E. Reilinger, R. Cakmak, T. Herring, H. Ozener, O. Lenk, and E. Tari (2009), Seven years of postseismic deformation following the $M = 7.4$ and $M = 7.2$, Izmit-Düzce, Turkey earthquake sequence, *J. Geophys. Res.*, *114*, B07403, doi:10.1029/2008JB006021.

Eyidogan, H., U. Guklu, Z. Utku, and E. Degirmenci (1991), Microseismic guide for major earthquakes of Turkey(1900–1988) Istanbul Technical University, Faculty of Mines, Publications of Geophysics Engineering Dept. 198 pp.

Galehouse, J. S., and J. J. Lienkaemper (2003), Inferences drawn from two decades of alignment array measurements of creep on faults in the San Francisco Bay region, *Bull. Seismol. Soc. Amer.*, *93*, 2415–2433.

Gomberg, J., and M. Ellis (1994), Topography and tectonics of the central New Madrid seismic zone: Results of numerical experiments using a three-dimensional boundary element program, *J. Geophys. Res.*, *99*, 20,299–20,310, doi:10.1029/94JB00039.

Gormus, K. S., S. H. Kutoglu, C. Mekik, H. Kemaldere, and E. Koksal (2013), Creep monitorings at Ismetpasa segment of North Anatolian Fault, International Symp. on Global Naviation Satellite System (ISGNSS) 2013, YTU Davutpasa Congress Centeer, 22–25 October 2013, Istanbul 13 pp. [Available at http://geomatik.beun.edu.tr/mekik/files/2013/11/NO-206-Cetin-Mekik-Creep-monitorings-at-Ismetpasa-segment-of.pdf.]

Kaneko, Y., Y. Fialko, D. T. Sandwell, X. Tong, and M. Furuya (2013), Interseismic deformation and creep along the central section of the North Anatolian fault (Turkey): InSAR observations and implications for rate and state friction properties, *J. Geophys Res. Solid Earth*, *118*, 316–331, doi:10.1029/2012JB009661.

Karabacak, V., E. Altunel, and Z. Cakir (2011), Monitoring aseismic surface creep along the North Anatolian fault (Turkey) using ground-based LIDAR, *Earth Planet. Sci. Lett.*, *304*, 64–70.

Ketin, I. (1957), The North Anatolian earthquake fault, *Istanbul Tech. Univ. Bull.*, *15*, 49–52 [in Turkish with English abstract].

Kondo, H., Y. Awata, Ö. Emre, A. Doğan, S. Özalp, F. Tokay, C. Yıldırım, T. Yoshioka, and K. Okumura (2005), Slip distribution, fault geometry, and fault segmentation of the 1944 Bolu-Gerede earthquake rupture, North Anatolian Fault, Turkey, *Bull. Seismol. Soc. Am.*, *95*, 1234–1249, doi:10.1785/0120040194.

Kondo, H., V. Özaksoy, and C. Yıldirim (2010), Slip history of the 1944 Bolu-Gerede earthquake rupture along the North Anatolian fault system: Implications for recurrence behavior of multisegment earthquakes, *J. Geophys. Res.*, *115*, B04316, doi:10.1029/2009JB006413.

Kutoglu, H. S., and H. Akcin (2006), Determination of 30-year creep on the Ismetpasa segment of the North Anatolian fault using an old geodetic network, *Earth Planet Space Lett.*, *58*, 937–942.

Kutoglu, H. S., H. Akcin, H. Kemaldere, and K. H. Gormus (2008), Triggered creep rate on the Ismetpasa segment of the North Anatolian fault, *Nat. Hazards Earth Syst. Sci.*, *8*, 1369–1373.

Kutoglu, H. S., H. Akcin, O. Gundogdu, K. S. Gormus, and E. Koksal (2010), Relaxation on the Ismetpasa segment of the North Anatolian fault after the Golcuk M_w = 7.4 and Duzce M_w = 7.2 shocks, *Nat. Hazards Earth Syst. Sci.*, *10*, 2653–2657.

Kutoglu, H. S., K. S. Gormus, T. Degouchi, E. Koksal, H. Kenaldere, and O. Gundogdu (2012), Can a creeping segment become a monitor before destructive major earthquakes, *Nat. Hazards*, *65*(21612173), 1369–1373.

Kutoglu, H. S., K. S. Gormus, T. Deguchi, E. Koksal, H. Kemaldere, and O. Gundogdu (2013), Can a creeping segment become a monitor before destructive major earthquakes?, *Nat. Hazards*, *65*, 2161–2173, doi:10.1007/s11069-012-0466-0.

Langbein, J., J. R. Murray, and H. A. Snyder (2006), Coseismic and initial postseismic deformation from the 2004 Parkfield, California, earthquake, observed by Global Positioning System, electronic distance meter, creepmeters, and borehole strainmeters, *Bull. Seism. Soc. Amer.*, *96*(4B), S304–S320, doi:10.1785/0120050823.

Lienkaemper, J. J., S. B. DeLong, C. J. Domrose, and C. M. Rosa (2016), Afterslip behavior following the M6.0, 2014 South Napa earthquake with implications for afterslip forecasting on other seismogenic faults, *Seismol. Res. Lett.*, *87*, 609–619, doi:10.1785/0220150262.

Lienkaemper, J. L., F. S. McFarland, R. W. Simpson, R. Bilham, D. A. Ponce, J. J. Boatwright, and S. J. Caskey (2012), Hayward Fault: Long-term Creep rates suggest a large locked patch controls the size and frequency of its large earthquakes, *Bull. Seismol. Soc. Amer.*, *102*(1), 2024–2034, February 2012 BSSA-D-11-00033R3.

Lindsey, E. O., Y. Fialko, Y. Bock, D. T. Sandwell, and R. Bilham (2014), Localized and distributed creep along the southern San Andreas Fault, *J. Geophys. Res. Solid Earth*, *119*, 7909–7922, doi:10.1002/2014JB011275.

McClusky, S., et al. (2000), Global Positioning System constraints on plate kinematics and dynamics in the eastern Mediterranean and Caucasus, *J. Geophys. Res.*, *105*, 5695–5719, doi:10.1029/1999JB900351.

Ozener, H., A. Dogru, and B. Turgut (2013), Quantifying aseismic creep on the Ismetpasa segment of the North Anatolian Fault Zone (Turkey) by 6 years of GPS observations, *J. Geodyn.*, *67*, 72–77.

Reilinger, R., et al. (2006), GPS constraints on continental deformation in the Africa-Arabia-Eurasia continental collision zone and implications for the dynamics of plate interactions, *J. Geophys. Res.*, *111*, B05411, doi:10.1029/2005JB004051.

Rousset, B., R. Jolivet, M. Simons, C. Lassere, B. Riel, P. Milillo, Z. Çakir, and F. Renard (2016), An aseismic slip transient on the North Anatolian Fault, *Geophys. Res. Lett.*, *43*, 3254–3262, doi:10.1002/2016GL068250.

Şaroğlu, F., and A. A. Barka (1995), Deprem Sonrası Devam Eden Uzun Dönem Yerdeğiştirmelerin Anlamı Ve Önemi. Nezihi Canitez Simpozumu, *Jeofizik Dergisi*, *9*(2), 339–343.

Schulz, S. S., G. M. Mavko, R. O. Burford, and W. D. Stuart (1982), Long-term fault creep observations in central California, *J. Geophys. Res.*, *87*, 6977–6982, doi:10.1029/JB087iB08p06977.

Taymaz, T., T. J. Wright, S. Yolsal, O. Tan, E. Fielding, and G. Seyitoğlu (2007), Source characteristics of the 6 June 2000 Orta Çankırı (central Turkey) earthquake: A synthesis of seismological, geological and geodetic (InSAR) observations, and internal deformation of the Anatolian plate, in The Geodynamics of the Aegean and Anatolia, edited by T. Taymaz et al, *Geol. Soc. Spec. Publ.*, *291*, 259–290.

Titus, S. J., C. DeMets, and B. Tikoff (2005), New slip rate estimates for the creeping segment of the San Andreas fault, California, *Geology*, *33*(3), 205–208, doi:10.1130/G21107.1.

Titus, S. J., C. DeMets, and B. Tikoff (2006), Thirty-five-year creep rates for the creeping segment of the San Andreas Fault and the effects of the 2004 Parkfield earthquake: Constraints from alignment arrays, continuous global positioning system, and creep-meters, *Bull. Seismol. Soc. Amer*, *96*(4B), 250–268, doi:10.1785/0120050811.

Wei, M., Y. Kaneko, Y. Liu, and J. J. McGuire (2013), Episodic fault creep events in California controlled by shallow frictional heterogeneity, *Nat. Geosci.*, *6*, 1–5.

Wesson, R. L. (1988), Dynamics of fault creep, *J. Geophys. Res.*, *93*, 8929–8950, doi:10.1029/JB093iB08p08929.

Erratum

In the originally published version of this article, Data Sets S1 and S2 were missing from the online Supporting Information. The files have since been added, and this version may be considered the authoritative version of record.